Available online at www.sciencedirect.com
ScienceDirect
C. R. Physique 8 (2007) 1100–1128
COMPTES RENDUS PHYSIQUE
http://france.elsevier.com/direct/COMREN/

Optical parametric sources for the infrared/Sources optiques paramétriques pour l'infrarouge

Infrared (2–12 μm) solid-state laser sources: a review

Antoine Godard

ONERA – Office national d'études et de recherches aérospatiales, chemin de la Hunière, 91761 Palaiseau cedex, France

Available online 7 November 2007

Abstract

The infrared domain is very attractive for many applications owing to two unique features: (i) it contains several atmospheric transparency windows, (ii) it corresponds to the 'molecular fingerprint' region of the electromagnetic spectrum where various molecules have strong rovibrational absorption lines. In many cases, these applications (e.g. laser surgery, trace gas monitoring, remote sensing, nonlinear spectroscopy, countermeasures, ...) require coherent light radiation as the one emitted by a laser source. In this context, the choice of the proper technology is a key issue. Depending on the selected application, it could be required the source to deliver tunable emission, narrow linewidth, nearly diffraction limited beam, pulsed or continuous-wave (CW) radiation, etc. This article briefly reviews the main technologies, restricted to CW and nanosecond pulsed sources emitting in the 2–12 μm range. The technologies considered include rare-earth and transition-metal doped bulk and fiber lasers, semiconductor lasers, and optical parametric sources. Pros and cons of these technologies are then briefly discussed in the context of several selected applications. ***To cite this article: A. Godard, C. R. Physique 8 (2007).***

Résumé

Sources laser solide infrarouge (2–12 μm) : une revue. Le domaine infrarouge est très intéressant pour de nombreuses applications grâce à deux caractéristiques particulières : (i) il contient plusieurs fenêtres de transmission de l'atmosphère, (ii) il correspond à la région 'd'empreintes digitales' du spectre électromagnétique où de nombreuses molécules présentent de fortes raies rovibrationnelles d'absorption. Dans de nombreux cas, ces applications (telles que la chirurgie laser, l'analyse de gaz, la détection à distance, la spectrocopie non linéaire, les contre-mesures) nécessitent de disposer de rayonnement cohérent tel que celui émis par une source laser. Dans ce contexte, le choix de la bonne filière est un paramètre clef. En fonction de l'application sélectionnée, il peut être requis que la source délivre un rayonnement accordable, une faible largeur de raie, un faisceau proche de la limite de diffraction, une émission continue ou impulsionnelle, etc. Cet article passe brièvement en revue les principales technologies, restreintes aux sources continues ou impulsionnelles nanoseconde émettant dans l'intervalle 2–12 μm. Les filières technologiques considérées incluent les lasers solide et fibre dopés aux ions terre-rare ou métal de transition, les lasers semi-conducteurs et les sources paramétriques optiques. Les avantages et les inconvénients de ces technologies sont ensuite discutés rapidement dans le contexte de quelques applications sélectionnées. ***Pour citer cet article : A. Godard, C. R. Physique 8 (2007).***

Keywords: Infrared; Laser; Rare-earth; Transition metal; Semiconductor laser; Quantum cascade laser; Optical parametric source

Mots-clés : Infrarouge ; Laser ; Terre-rare ; Métal de transition ; Laser à semi-conducteur ; Laser à cascade quantique ; Source paramétrique

E-mail address: antoine.godard@onera.fr.

1631-0705/$ – see front matter
doi:10.1016/j.crhy.2007.09.010

1. Introduction

Coherent light sources emitting infrared radiation in the 2–12 μm range are very useful for many applications that rely on the two unique features of this spectral region: (i) well-known atmospheric transparency windows are located in this wavelength range; (ii) various molecules have strong rovibrational absorption lines in this 'molecular fingerprint' region of the electromagnetic spectrum. Among these applications, one should mention laser surgery, trace gas monitoring, remote sensing, nonlinear spectroscopy, countermeasures, ...

Depending on the application, the required properties of the coherent light source can vary considerably. For instance, some applications require high power tunable emission regardless of the spectral purity while other applications require pulsed narrow-linewidth radiation in a nearly diffraction limited beam. The choice of the most relevant technology for a given application is thus a critical issue.

The purpose of this article is to briefly review some of the most advanced infrared solid-state laser technologies and to discuss their relative capabilities in the context of selected applications. Because it is not possible in a brief review to do justice to all the achievements obtained over the past years, we focus on the last results obtained in continuous-wave (CW) and nanosecond pulsed regimes, in the 2–12 μm range, for the following technologies:

- crystalline and fiber rare-earth doped laser (Er, Tm, Ho);
- vibronic solid-state laser (Cr, Fe);
- antimonide-based heterojunction laser diodes;
- quantum cascade lasers;
- optical parametric sources.

For a more complete review, the reader should, for example, refer to [1] and references therein.

Comparison between the above mentioned technologies is then discussed in the context of several applications. The discussion is organized considering two sub-spectral ranges: 2–3 μm where the emission spectra of most of the technologies are included and 3–12 μm where the choice is limited to quantum cascade lasers and parametric sources. Following this comparative study we draw our general conclusions. In particular, we find out that, similarly to visible and near-infrared laser sources where several technologies are coexisting, most of the reported technologies provide unique properties compared to the others, making them the solution of choice for a given class of applications.

2. Crystalline and fiber rare-earth doped lasers

2.1. Tm^{3+} based lasers

Tm-doped lasers are well known to provide tunable emission in the 1.9–2 μm spectral using the $^3H_4 \rightarrow {}^3H_6$ transition in a quasi-three level scheme (see Fig. 1). The development of 2-μm Tm-doped lasers has been driven by many applications in medical, commercial, and military technologies. The strong absorption of radiation by water and human tissues in the specific interval between 1.92 and 1.94 μm is attractive for laser surgery, while the low atmospheric absorption and 'eye-safe' properties make this system useful for materials processing, range-finding, remote sensing, and other applications. Indeed, in this spectral region, several atmospheric components, such as H_2O, CO_2, and NO_2, have many absorption lines that can be exploited in differential absorption lidar (DIAL) systems. In addition, 2-μm lasers can be useful for pumping Ho-based and Cr-based lasers as well as mid-infrared optical parametric oscillator materials for which 1-μm radiation cannot be used.

Diode-pumped CW as well as pulsed laser operations have been demonstrated with both bulk and fiber lasers. Furthermore, very efficient pumping schemes with slope efficiency exceeding the Stokes limit can be achieved at high thulium doping concentration (>5%) thanks to cross-relaxation energy transfer between Tm^{3+} ions. During the cross-relaxation energy transfer process, two ground-level thulium ions can be excited to the upper lasing level by absorbing only one pump photon near 790–800 nm, which means one excited Tm^{3+} ion at the $^3F_4$ level generates two Tm^{3+} ions at the $^3H_4$ upper laser level.

Thanks to the cross relaxation process, a Tm-doped germanate glass fiber CW laser emitting 64 W at 1.9 μm from 100 W at 800 nm (68% slope efficiency, significantly higher than the Stokes limit of 42%) has been recently reported (see Fig. 2) [2]. As much as 112 W at 2.03 μm with a close to diffraction limited beam quality ($M^2 < 1.5$) was also

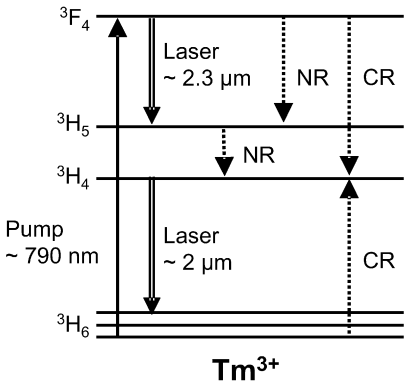

Fig. 1. Partial energy-level diagram of Tm^{3+} ion. NR and CR represent nonradiative decay and cross-relaxation, respectively.

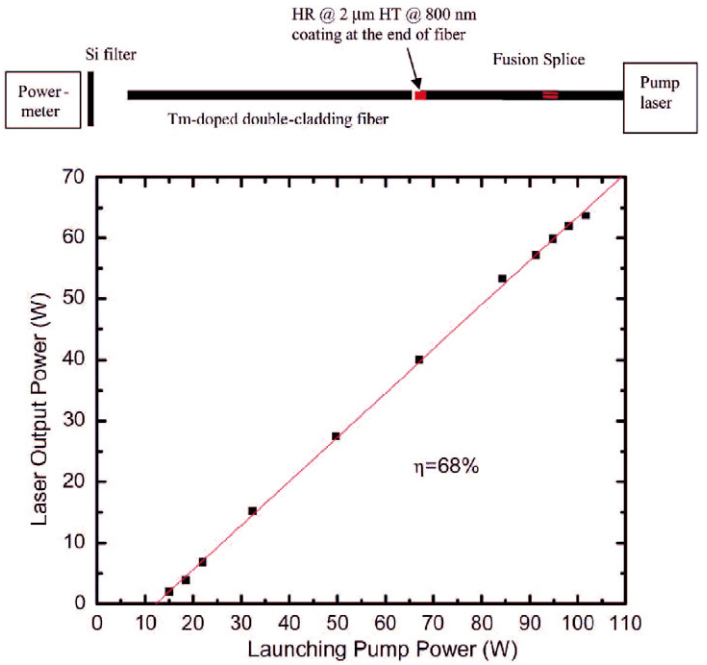

Fig. 2. Schematic of a thulium-doped germanate fiber laser setup (top) and laser output power versus launching pump power (bottom), after [2].

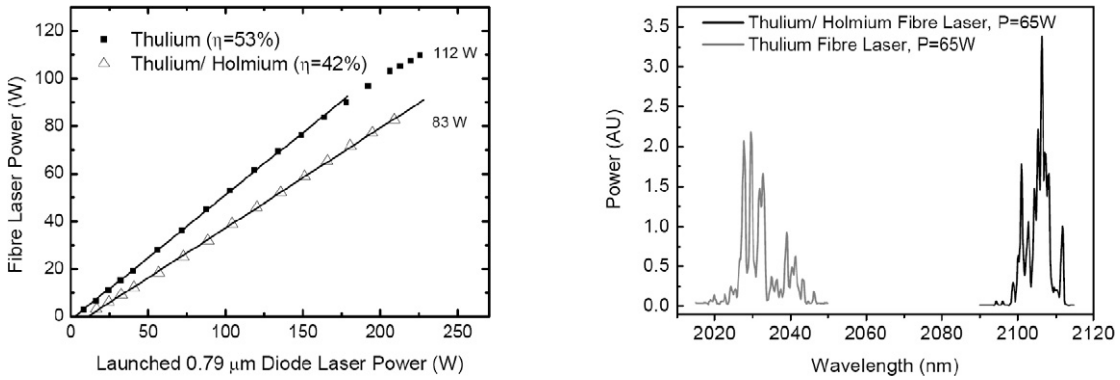

Fig. 3. Output power from silica fibre lasers measured as a function of the launched pump power (left) and spectral output of the Tm^{3+}/Ho^{3+} and Tm^{3+} fibre lasers (right), after [3].

recently demonstrated with a Tm-doped CW silica fiber laser pumped by laser diodes emitting at 793 nm with slope efficiency of 53% (see Fig. 3) [3]. Even higher output powers, up to 150 W, are available with a diffraction limited beam ($M^2 < 1.05$) from commercial CW fiber laser at the price of a lower efficiency because of a different pumping scheme where a pump wavelength of 960 nm is used (no 2-for-1 cross relaxation process) [4].

High power emission has also been demonstrated in CW bulk lasers. For instance, as much as 120 W CW output power has been obtained at 2.01 µm in a diode-pumped Tm:YAG laser using the side-pumped end-capped rod geometry and the compound parabolic concentrators pump delivery. However, such high power level was obtained at the expense of the beam quality ($M_x^2 = 21$ and $M_y^2 = 14$) [5]. More recently, another paper reported on 28 W of polarized CW output power with $M^2 < 1.3$ beam quality from a Tm:YLF laser using a novel side-pumped slab geometry.

In Q-switched pulsed regime, the reported average power also reach the 30 W level in bulk lasers with a nearly diffraction limited beam [7]. The pulse duration was typically 100 ns with a repetition rate of several kilohertz using

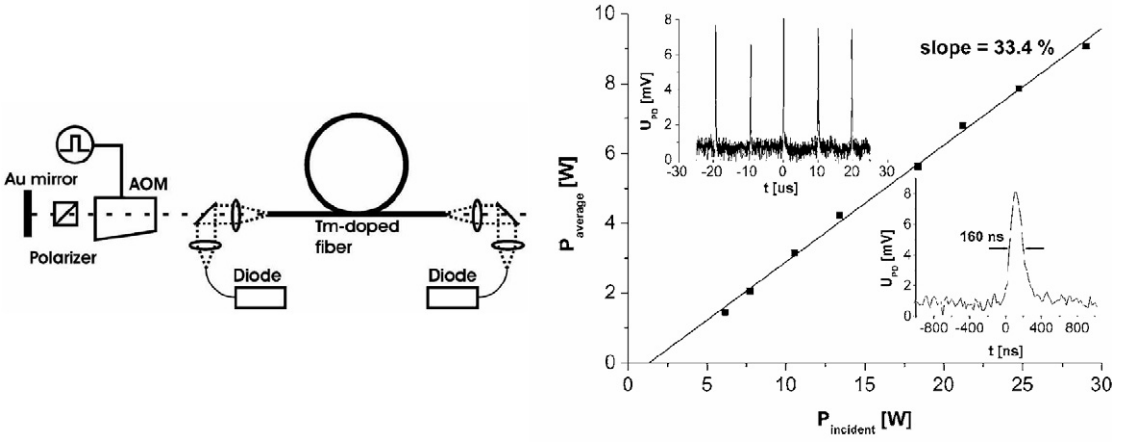

Fig. 4. Schematic of a Q-switched Tm-doped double-clad fluoride fiber laser (left) and average output power versus incident pump power at 100 kHz rep. rate (the insets show the pulses at maximum pump power) (right), after [8].

Table 1
Examples of demonstrated tunability in Tm-doped lasers

Active material	Tuning range	Tuning width	Ref. (year)
Tm:YAG	1.87–2.16 μm	290 nm	[11] (1990)
Tm:YSGG	1.84–2.14 μm	300 nm	[11] (1990)
Tm:$YAlO_3$	1.93–2 μm	70 nm	[12] (1995)
Tm:Y_2O_3	1.93–2.09 μm	160 nm	[13] (1999)
Tm:Sc_2O_3	1.93–2.16 μm	230 nm	[13] (1999)
Tm:silica fib.	1.86–2.09 μm	230 nm	[14] (2002)
Tm:YLF	1.91–2.07 μm	160 nm	[6] (2002)
Tm:$GdVO_4$	1.86–1.99 μm	130 nm	[15] (2002)
Tm:silica fib.	1.72–1.97 μm	250 nm	[16] (2006)
Tm:BaY_2F_8	1.78–2.03 μm	245 nm	[9] (2006)

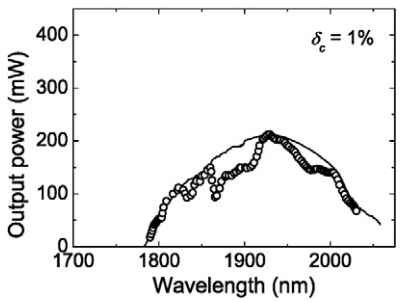

Fig. 5. Tunability curve of a Tm:BaY_2F_8 laser, measured at 1 W incident pump power with a 1% transmission output coupler, after [9].

Tm:$YAlO_3$ as a laser material. The investigation of high repetition rate fiber laser is more recent than for bulk devices. In [8], a diode-pumped Q-switched Tm-doped double-clad fluoride fiber laser is reported providing up to 90 μJ pulse energy (160 ns, 100 kHz, i.e., 9 W of average power) using a D-shape pump cladding and an inner fiber geometry that stabilizes the fundamental mode and enhances the energy storage capability of the fiber (see Fig. 4).

Another important feature of Tm-doped lasers is the possibility of continuous tuning. In the 1.9–2 μm spectral region, various tuning ranges have been demonstrated as a function of the host matrices as reported in Table 1. As an example, Fig. 5 presents a wide 245 nm tunability, recently demonstrated in Tm:BaY_2F_8 [9].

Tunable laser operation in the 2.2–2.4 μm spectral range can also be obtained by use of $^3F_4 \rightarrow {}^3H_5$ transition. Conversely to $^3H_4 \rightarrow {}^3H_6$ transition, the cross-relaxation process is detrimental because it induces depopulation

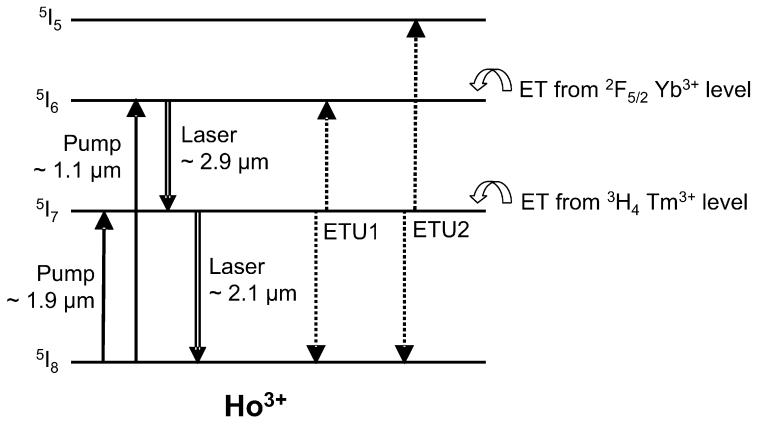

Fig. 6. Partial energy-level diagram of Ho^{3+} ion. ETU and ET represent energy transfer upconversion and energy transfer from sensitizer ion (here Tm^{3+} or Yb^{3+}), respectively.

of the upper laser level $^3F_4$. Therefore, the operation in the 2.3 µm range requires a low concentration of Tm^{3+}, typically <2%. Among the much more limited literature devoted to Tm-based laser emitting at 2.3 µm, one should mention the demonstration of tunability in the whole 2.2–2.46 µm range with a maximal output power of 200 mW in Tm:YLF [10].

2.2. *Ho^{3+} based lasers*

Infrared laser oscillation using Ho^{3+} as the active ion can be achieve in the 1.95–2.15 µm range with the $^5I_7 \rightarrow {}^5I_8$ transition and in the 2.85–3.05 µm range with the $^5I_6 \rightarrow {}^5I_7$ transition (see Fig. 6).

For the same motivations as Tm-based lasers, the development of pulsed 2-µm Ho lasers has remained a topic of particular interest for many years, due to a number of possible applications such as coherent LIDAR, atmospheric sensing, or as pump source for optical parametric oscillator operating in the mid-infrared region, including $ZnGeP_2$ OPOs for countermeasure applications. In addition, CW 2-µm lasers have significant potential in laser welding of transparent plastic materials as well as laser surgery and therapy [17].

Laser emission in the 2-µm range requires optical pumping of Ho^{3+} ion at 1.9 µm. As a consequence Ho^{3+} ion alone cannot be pumped by standard commercially available high-power laser diodes. Tm–Ho co-doping is then required to achieve direct diode pumping. In this case, Tm^{3+} acts as a sensitizer ion that strongly absorbs the pump light and subsequently transfers the absorbed energy to the active ion, i.e. Ho^{3+}. Thanks to these nonradiative energy transfer processes in the Tm–Ho system, very high pulse energies (1.1 J/pulse at 2 Hz rep. rate and 187 ns pulse duration) have been obtained in Q-switched mode at 2.053 µm with a 1.4 times transform-limited beam quality in a diode-pumped Ho,Tm:LuLF laser. Such system was based on a side-pumped rod configuration in a master-oscillator-power-amplifier (MOPA) architecture developed for future spaceborne coherent Doppler wind lidar (see Fig. 7) [18]. However, average power scaling of lasers that relies on the Tm–Ho system in a diode-pumped CW and repetitively Q-switched mode of operation is rather difficult because of upconversion losses at high pump levels and the reversible transfer between the Tm and the Ho first excited states [19]. The combination of these effects produces a very large thermal load, which severely limits performance at the high pump levels that are needed to achieve gain at room temperature.

In this context, direct laser pumping of the Ho $^5I_7$ manifold is preferred to circumvent the average power limitations of the sensitized Tm–Ho system. Indeed, direct laser pumping (with 1.9-µm radiation) of the quasi-two-level Ho offers several advantages over the sensitized Tm–Ho system: low quantum defect (1.9 to 2 µm), elimination of energy transfer (no sensitizer ion used), reduced upconversion losses (linearity of gain versus pump intensity), high short-pulse extraction efficiency, and reduced sensitivity of gain versus temperature. The advantages combined produce a 2-µm laser capable of high power scaling and high-energy output (lifetime reduction under intense pumping is lower than sensitized Tm-Ho). This kind of scheme was implemented by several groups to produce average power in the 10 W level in Q-switched mode at several kilohertz repetition rates with a good beam quality, mainly for ZGP

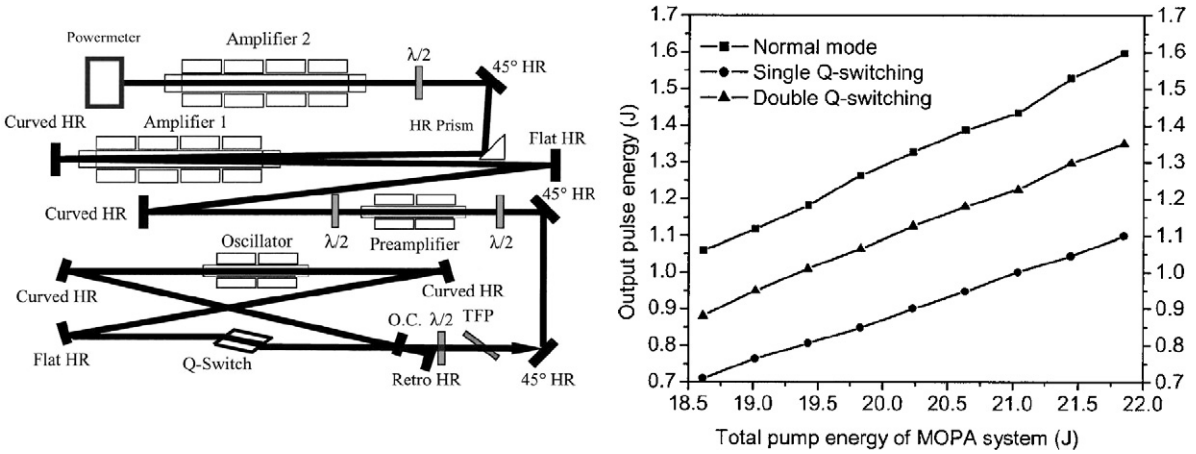

Fig. 7. Schematic of a diode-pumped 2 μm Ho,Tm:LuLF MOPA system (left) and output energy performance at 2-Hz rep. rate (right), after [18].

OPO pumping [20,21]. Direct pumping by 1.9-μm laser diodes has also been demonstrated, achieving up to 0.7 W of CW output [22]. The highest power level demonstrated with bulk Ho-based lasers have been obtained by use of a commercial Tm-doped fiber laser as a pump source. From 100 W at 1.9 μm, as much as 42 W were thus delivered at the output of an Ho:YAG laser in CW regime as well as 28 mJ pulses at 1 kHz rep. rate or 45 mJ pulses at 400 Hz in Q-switched regime [23].

Nevertheless, the sensitized Tm–Ho system remains promising for fiber architecture that allows effective heat dissipation with minimal heat-sinking requirement. Indeed, as much as 83 W of CW power at 2.1 μm in a diffraction limited beam have been obtained from 200 W at 793 nm by use of a Tm,Ho co-doped water-cooled silica fiber system (see Fig. 3) [3].

Ho-based lasers emitting in the 3-μm range are less common. The main limiting issue is the population bottleneck effect that occurs with the $^5I_6 \rightarrow {}^5I_7$ transition which is a self-terminated transition. Indeed, the $^5I_6$ manifold has a longer lifetime than the $^5I_7$ manifold leading to population accumulation in the lower laser level during oscillation.

The saturation of the $^5I_6 \rightarrow {}^5I_7$ transition can be suppressed by cascade lasing or lower manifold deactivation. Cascade lasing consists in the oscillation on both transitions of the Ho^{3+} in the same resonator. Such cascade oscillation scheme has been demonstrated for instance in Cr,Yb,Ho:YSGG [24]. Compared to cascade lasing, however, the use of a deactivator, e.g., Pr^{3+} (see Fig. 8 (a, left)), reduces the complexity of the laser resonator and provides single-emission output. In this way, up to 2.5 W CW output (single-transverse-mode) have been obtained at 2.86 μm by use of Pr–Ho co-doped fluoride fiber pumped by Yb-based MOPA fiber system emitting 9 W (see Fig. 8) [25].

Direct diode pumping has also been demonstrated by use of Yb^{3+} as a sensitizer. Hence, a pulsed diode-pumped Ho,Yb:YSGG laser has been realized at 2.84 μm, achieving 10 mJ output energy with 2.5% efficiency [26].

2.3. Er^{3+} based lasers emitting around 3 μm

Er^{3+} is well know as an active ion for its laser transition $^4I_{13/2} \rightarrow {}^4I_{15/2}$ providing emission around 1.55 μm. Laser oscillation can also be obtained in the mid-infrared in the 2.58–2.94 μm range (depending on the host material) using the $^4I_{11/2} \rightarrow {}^4I_{13/2}$ transition that can also be diode pumped at 960 nm (see Fig. 9). The related laser emission coincides with O–H vibration in water and is thus strongly absorbed by biological tissues within less than a micrometer. This feature makes Er-based laser very attractive for medical applications such as laser surgery and ophthalmology [17].

As for the 3-μm Ho-based laser, the Er^{3+} $^4I_{11/2} \rightarrow {}^4I_{13/2}$ laser transition is self-terminated leading to population bottleneck issues. Nevertheless, efficient operation has been demonstrated in CW as well as pulsed regimes with Er-based laser despite this detrimental feature.

In the CW regime, the largest output powers have been obtained with fiber-laser architectures. For instance, as much as 9 W transverse-fundamental-mode CW output at 2.78 μm have been recently obtained from a 4-m heavily erbium-doped ZBLAN double-clad fiber laser with a launched pump power of 42.8 W from a collimated 975 nm

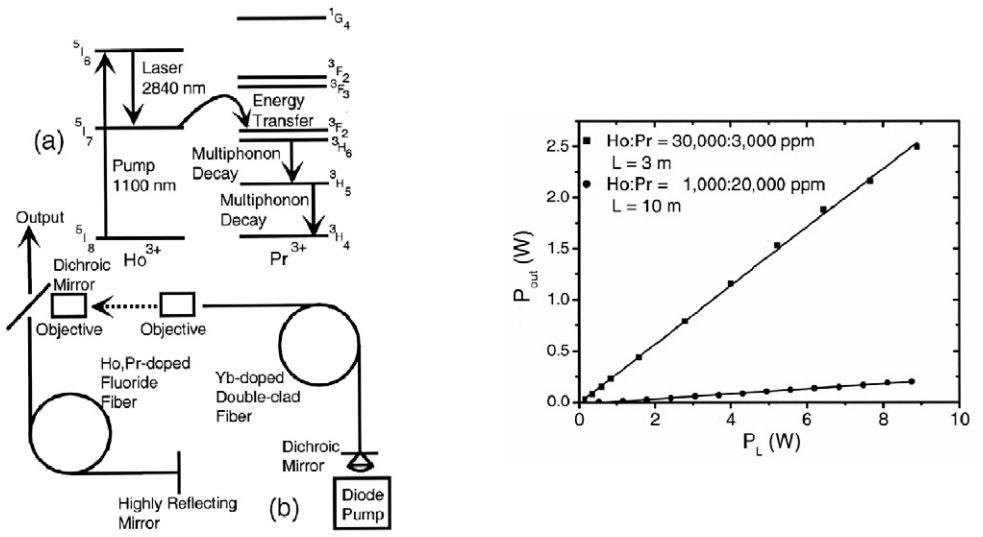

Fig. 8. Schematic diagram of the energy levels relating to Ho^{3+}, Pr^{3+}-codoped glass showing the major processes relevant to the fiber laser (a, left), the experimental setup (b, left) and measured output power as a function of the launched pump power from two Ho^{3+}, Pr^{3+}-codoped ZBLAN fiber lasers, each with a fiber having different dopant concentrations (right), after [25].

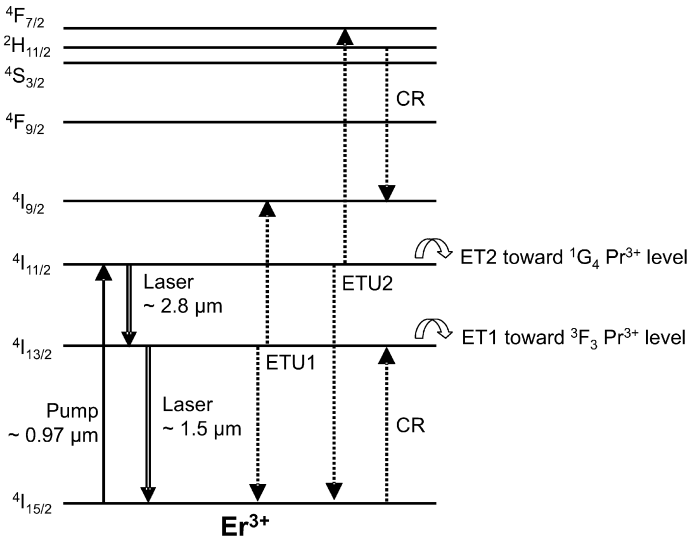

Fig. 9. Partial energy-level diagram of Er^{3+} ion. CR, ETU, and ET represent cross-relaxation, energy transfer upconversion and energy transfer to deactivator ion (here Pr^{3+}), respectively.

laser diode array (see Fig. 10) [27]. This high CW power was obtained by use of the energy-transfer upconversion process between Er and Er ions that occurs at high dopant concentration (Er^{3+} concentration of 6 mol.%). CW power demonstrated with bulk Er-based lasers is more limited: 4 W have been obtained at 2.81 μm with a diode-pumped Er:YLF laser using a sealed cavity purged by dry nitrogen to avoid water vapor absorption [28]. In the same work, tunable operation was also achieved over several discrete lines (2716–2717 nm, 2772–2773 nm, 2797–2798 nm, 2807–2809 nm) inserting a quartz birefringent filter in the laser cavity with a smaller efficiency (power limited to 1.3 W, see Fig. 11).

In the pulsed regime, flash-pumped architecture have been implemented to produce high energy pulses at low repetition rate. Hence, 137 mJ (90 ns duration and 3 Hz rep. rate) at 2.94 μm have been obtained from an actively Q-switched Er:YAG pumped by a single xenon flashlamp (see Fig. 12) [29]. For a diode pumping, pulses of 5.5 mJ (19 ns duration, 10 Hz rap. rate) have been obtained in Er:YLF and Er:YSGG with $M^2 = 2.7$ [30].

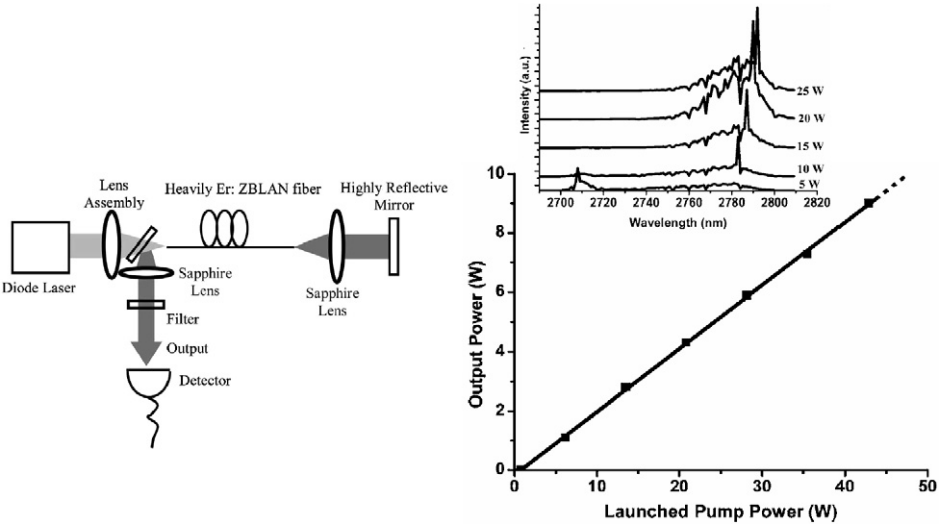

Fig. 10. Schematic of a high-power heavily Er doped ZBLAN double-clad fiber laser (left) and output power as a function of launched pump power (the inset shows the output spectra at different pump powers) (right), after [27].

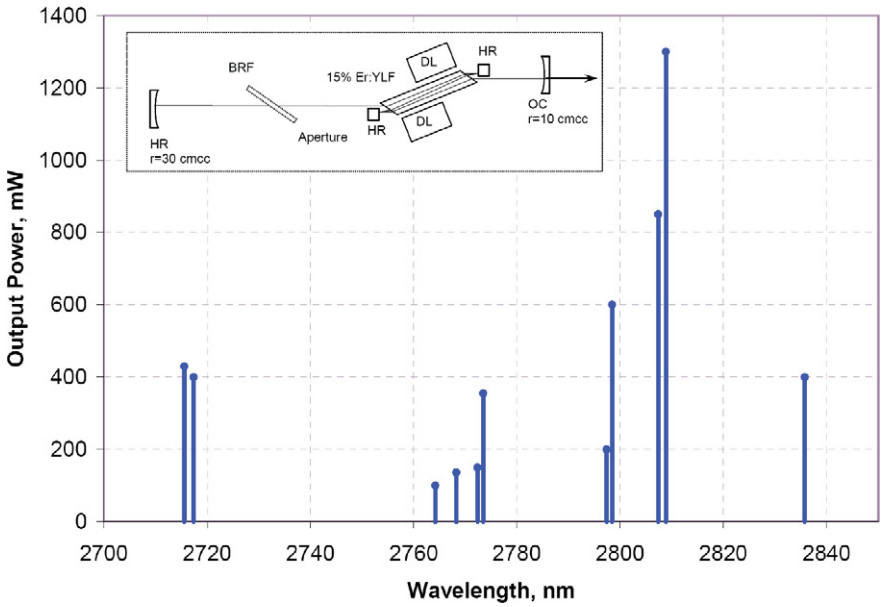

Fig. 11. Output power as a function of emitted wavelength for a BRF-tuned Er:YLF laser (the insert shows a schematic layout of the side-pumped Er:YLF laser, with extended resonator and BRF tuner), after [28]. BRF corresponds to an intracavity, single-plate, Brewster-angle, quartz birefringent filter.

3. Bulk transition metal doped lasers

3.1. Cr^{2+} based lasers

Cr^{2+}-doped II–VI compounds are laser materials with large emission bandwidths in the 2–4 μm range [31,32]. These lasers belong to the vibronic laser family where broad absorption and emission bands are obtained thanks to the strong coupling between the crystalline field and the optical electrons of the transition metal ions that are located in 3*d* outer shells. The association of transition metal ions with semiconductor host matrices leads indeed to specific optical properties whose detailed reviews can be found for example in [32] or [33]. A schematic energy diagram of Cr ions in

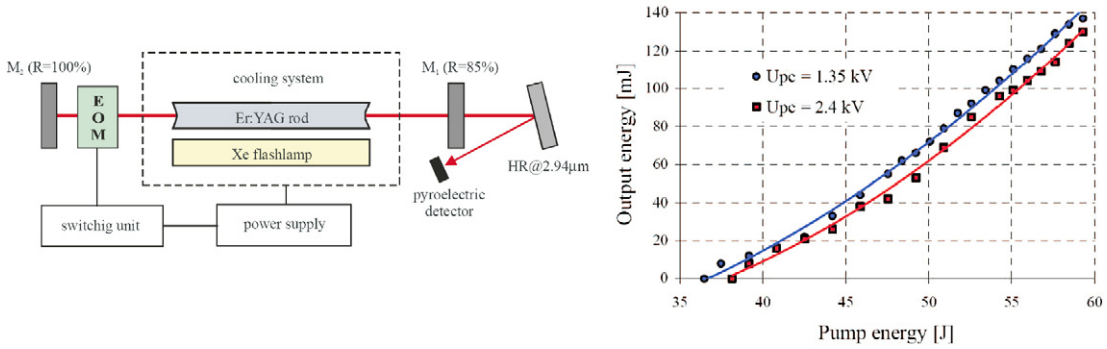

Fig. 12. Schematic of a Pockels cell Q-switched Er:YAG laser (left) and pulse output energy as a function of pump energy for two values of voltage applied to Pockels cell (U_{pc}) (right), after [29].

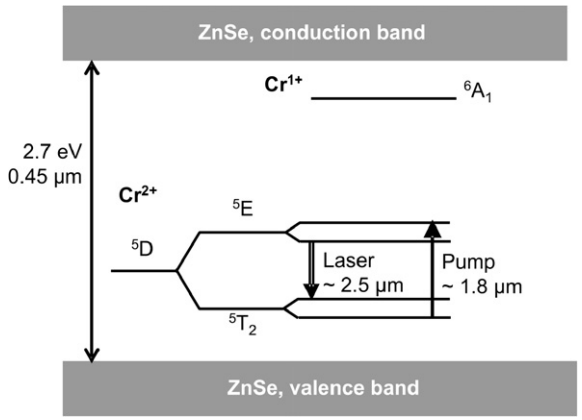

Fig. 13. Partial energy-level diagram of Cr^{2+} ion in ZnSe.

ZnSe is shown in Fig. 13. This figure shows that Cr^{2+} energy levels are located inside ZnSe band gap ($E_g = 2.7$ eV). The lowest free-ion ^5D state of Cr^{2+} is split by the crystal field into excited orbital doublet ^5E and a ground-state orbital triplet $^5T_2$. Both the orbital triplet ground- and the orbital doublet excited states are further split by several interaction: coupling with lattice vibration modes (Jahn Teller effect), first and second order spin–orbit couplings.

Cr^{2+}:ZnSe is surely the most famous among these Cr^{2+}-doped II–VI compound lasers. As shown by Fig. 14, Cr:ZnSe exhibits a broad absorption band centered at 1800 nm and it can be pumped by various pump sources including Tm-doped lasers emitting at 1.9 μm [34], Er-doped fiber laser emitting at 1.55 μm [35], or infrared laser diodes [36]. Efficient operation can be obtained with Cr:ZnSe thanks to the small quantum defect with broadband room-temperature operation leading to broad continuous tuning. Indeed, as shown by Fig. 15, record ultrabroad continuous tuning was achieved in the 1880–3100 nm range with four different sets of cavity optics [37]. One should also note that the extremely broad gain makes Cr:ZnSe especially attractive for ultrashort pulse generation (80 fs pulses were recently demonstrated [38]).

Due to relatively high thermal lensing the maximal output power is currently limited to 1.8 W in TEM_{00} mode CW regime [39]. However, based on the analysis of the mechanical, thermal, spectroscopic, and laser properties of Cr:ZnSe, the output powers over 10 W in CW regime are envisioned [33].

Efficient nanosecond pulsed operation requires the use of pulsed pump sources because of the short excited level lifetime limited to 6 μs. Nevertheless, more powerful Cr:ZnSe lasers have been implemented in pulsed regime, with as much as 18 W of average output power at 30 W absorbed power pumped by the Q-switched Tm:YALO laser at 7-kHz repetition rate (see Fig. 16) [40]. In this experiment tunability between 2.1–2.85 μm was achieved at up to 10 W output power by use of an intracavity acousto-optical filter and the beam quality was characterized by $M^2 = 1.85$.

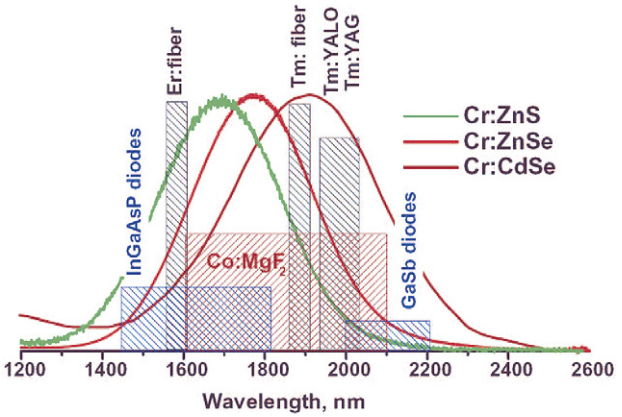

Fig. 14. Absorption spectra (in relative units) and possible pump sources for Cr^{2+}-doped II–VI media, after [32].

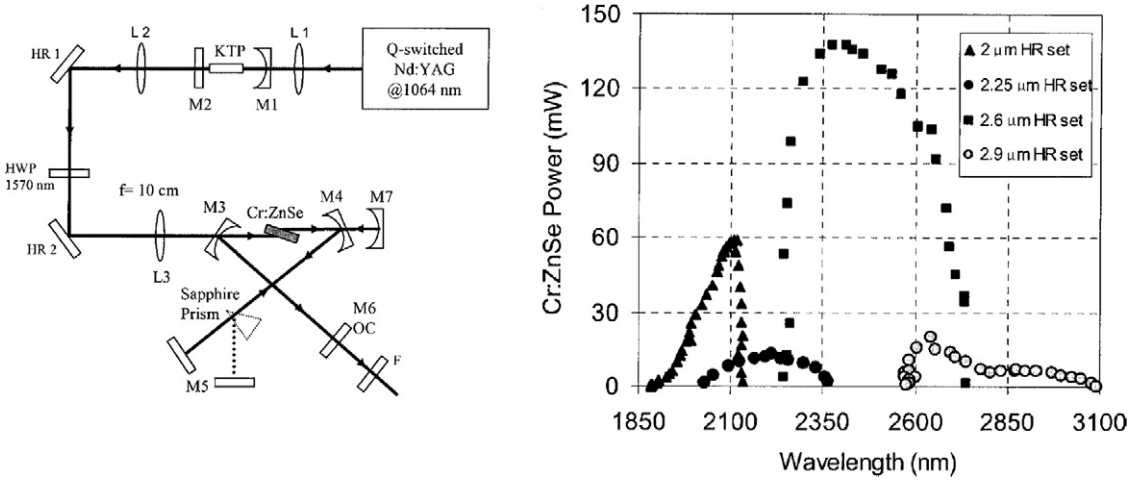

Fig. 15. Schematic of a tunable gain-switched Cr^{2+}:ZnSe laser at 1 kHz rep. rate (left). Full tuning range between 1880 and 3100 nm, taken with four different mirrors sets, available Nd:YAG pump power was about 1.8 W for all cases (right), after [37].

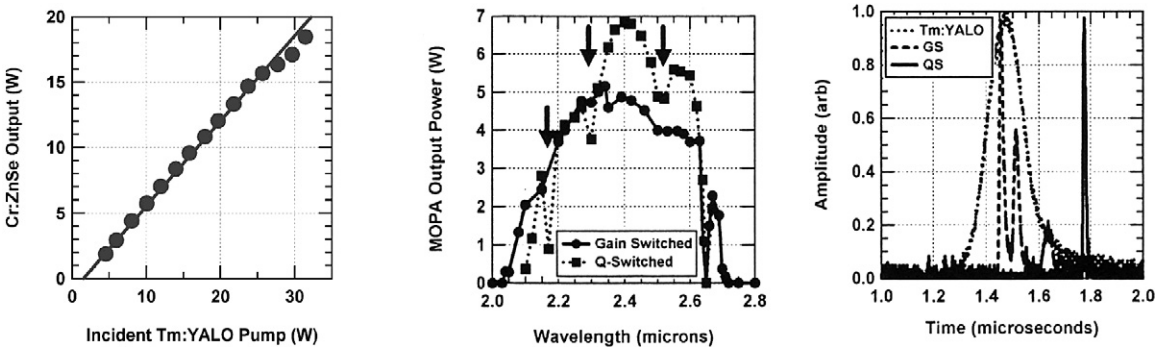

Fig. 16. Output power of a Cr:ZnSe power oscillator as a function of Tm:YALO pump power (left), Cr:ZnSe MOPA output power as a function of wavelength for both gain-switched and Q-switched operation (middle) and, temporal pulse profiles of Tm:YALO pump laser with the gain-switched and Q-switched MOPAs (right), after [40].

Cr:ZnSe lasers are thus very interesting as affordable, compact, room-temperature operational and broadly tunable mid-IR laser sources for use in a variety of remote sensing applications [41,42]. Cr:ZnSe can also be used for mid-IR OPO pumping such as ZGP- or CdSe-based OPOs [43,44].

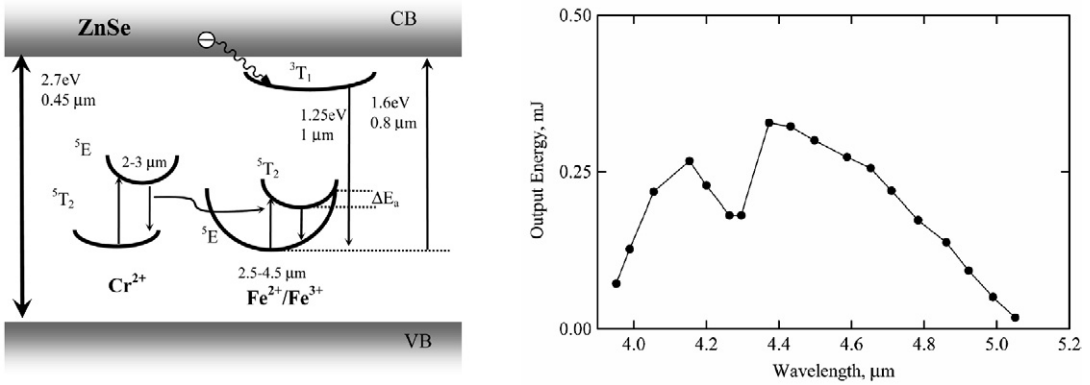

Fig. 17. Schematic energy diagrams of Fe and Cr ions in ZnSe (left) and tuning curve of room-temperature Fe:ZnSe laser with intracavity prism obtained at absorbed pump energy of 4.5 mJ (right), after [47].

In order to get Cr:ZnSe lasers even more compact, challenging research is currently oriented toward electrical pumping of a Cr:ZnSe laser. Recently, first observations of the room-temperature mid-IR electroluminescence of Cr^{2+}:ZnSe has been demonstrated by two groups [45,46]. Such results paves the way to electrically pumped laser action.

3.2. Fe^{2+} based lasers

Doping II–VI compounds with Fe^{2+} ions instead of Cr^{2+} ions provides laser emission at longer wavelengths in the 4–5 µm spectral region (see Fig. 17 (left)). However, mid-IR transitions in the Fe:ZnSe crystal have multiphonon quenching at room temperature that strongly limit lasing capabilities of this material. Nevertheless, efficient room-temperature Fe:ZnSe laser oscillation was recently achieved in pulsed regime using a 2.94-µm 60-ns pulse duration passively-Q-switched Er:YAG laser as a pump source [47]. With 4.5 mJ of incident pump energy, maximum output energy and slope efficiency were 0.37 mJ and 13%, respectively. The threshold absorbed pump energy was 1.4 mJ. The output spectrum of the Fe:ZnSe laser was then continuously tuned over the 3.95–5.05 µm spectral range (see Fig. 17 (right)).

4. Antimonide-based heterojunction laser diodes

In the 2–3 µm wavelength region, strained multi-quantum-well laser diodes based on the GaIn(As)Sb/AlGaAnSb system appear as the more established semiconductor laser technology [48]. Since the laser operation relies on interband transition, the emitted wavelength of these interband semiconductor lasers depends on the selected alloy composition, as illustrated by Fig. 18. Despite the limitation of carrier lifetime due to the Auger effect which strongly reduces the efficiency for wavelengths longer than 2 µm, these lasers can operate in CW regime at room temperature over the whole 1.9–2.7 µm range [49].

Maximal power level demonstrated in CW regime near room temperature are summarized in Fig. 19. From single broad area emitters, average powers of around 1 W have been demonstrated in the full 1.9–2.5 µm range [49–54]. In order to realize efficient optical pump sources for laser systems emitting in the 2–3 µm wavelength range and related applications, such as infrared countermeasures, diode laser arrays or bars have also been implemented with demonstrated output power in the 10–20 W range [54,55]. The maximal output power of 16.9 W (at 1.9 µm) has

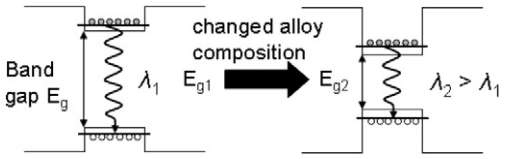

Fig. 18. Simplified band diagram illustrating that interband transitions depend primarily on the quantum-well alloy composition.

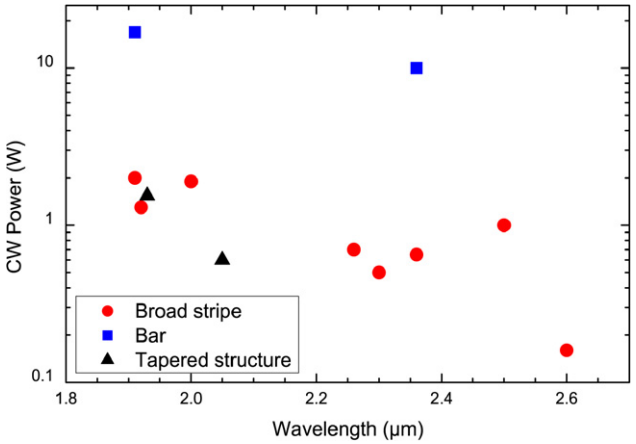

Fig. 19. Maximal power level from antimonide-based heterojunction laser diodes demonstrated in CW regime near room temperature. Data collected from [49–57].

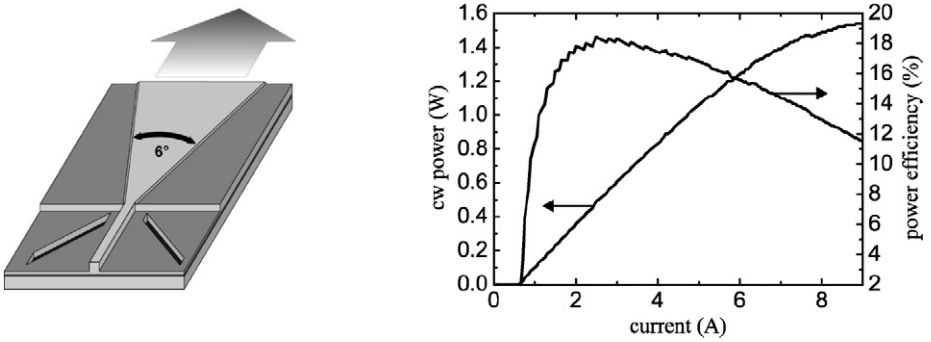

Fig. 20. Schematic of a GaSb-based tapered diode laser (the length of the ridge section is 500 μm, while the length of the tapered section is 2000 μm and the taper angle amounts to 6°) (left) and CW output power and power conversion efficiency versus current while the heat sink temperature was set to 20 °C (right), after [57].

been obtained from linear broad-area laser arrays comprising 19 emitters on a 1-cm-wide bar [55]. The emitters had a stripe-width of 150 μm and a pitch of 500 μm.

High brightness light sources have also been realized using tapered laser structures [56,57]. Hence, up to 1.5-W nearly diffraction-limited ($M^2 \sim 1.5$) power has been obtain by use of GaSb-based tapered diode lasers emitting at 1.93 m with a narrow waveguide design [57] (see Fig. 20). Arrays of tapered lasers have also been realized but CW operation at room temperature has not been demonstrated with this type of bar so far [58].

At lower output power, tunable and narrow linewidth lasers for spectroscopic sensing have also been implemented using various usual semiconductor laser structures. For instance, tunability with more than 10 mW in the full 2.2–2.4 μm range was obtained by use of an external cavity design as illustrated by Fig. 21 [59]. Single mode emission near 2.4 μm was also demonstrated using integrated devices such as distributed feedback (DFB) laser [60]. In this work, the emission wavelength of the DFB lasers could be tuned from 2.339–2.392 μm depending on the grating pitch, the output powers were of up to 8.5 mW per facet, and the side-mode suppression ratio was of 33 dB (see Fig. 22).

5. Quantum cascade lasers

The general principles of operation of quantum cascade lasers (QCLs) are presented here in a very simplified way. More detailed descriptions of the principal features of QCLs can be found for instance in [61] or [62].

In contrast to semiconductor laser diodes, initial and final states of the laser transition in quantum cascade lasers (QCLs) are in the conduction band. These distinct states inside the same band (referred as subbands) arise from

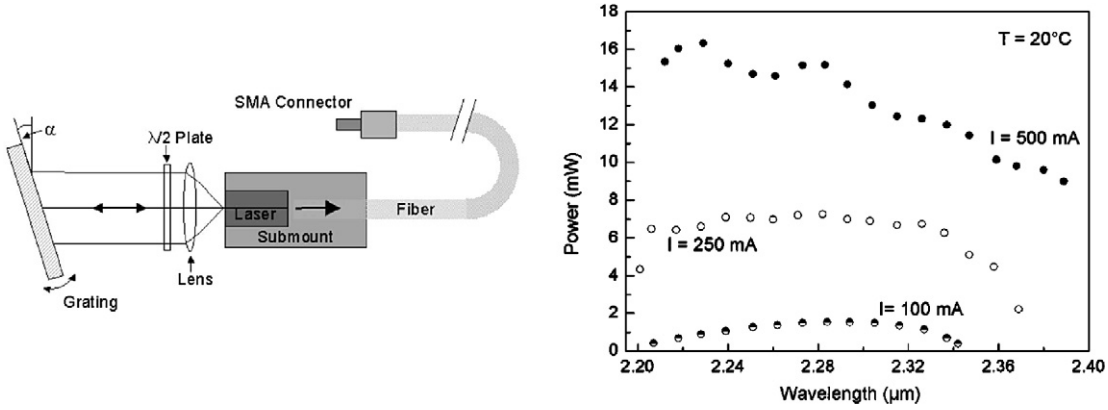

Fig. 21. Schematic of a tunable external cavity GaSb-based diode laser in Littrow-configuration (left) and wavelength-dependence of the output power for three different injection operating currents (right), after [59].

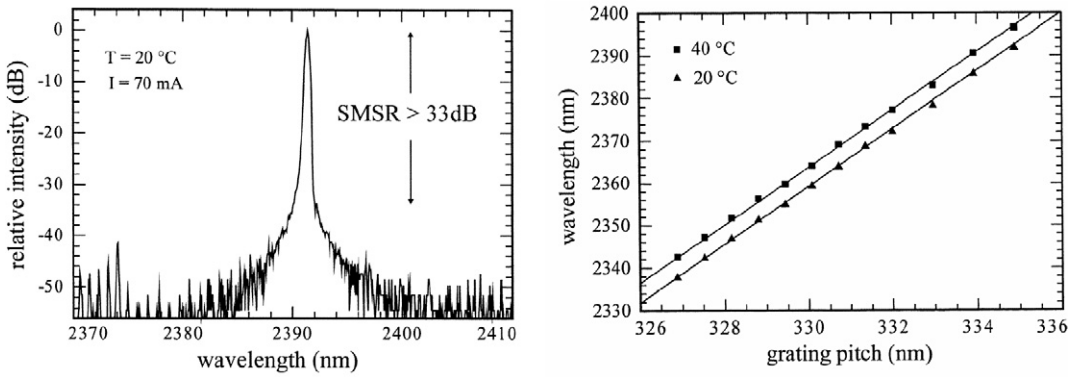

Fig. 22. CW operation spectrum of a laterally coupled 800 μm × 4 μm GaSb-based DFB laser with facets as cleaved (left) and control of the emission wavelength by variation of the grating period, measured under CW operation at 20 and 40 °C (right), after [60].

the quantization of electronic states due to the small sizes of semiconductor heterostructures (see Fig. 23). These transitions are commonly denoted as intersubband transitions. As a consequence, only one type of carrier (typically electrons) is involved in QCLs. This property fundamentally differentiates QCLs (unipolar devices) from laser diodes (bipolar devices which involve electrons and holes). The other fundamental feature of QCLs is the multistage cascade scheme where electrons are recycled so as to generate an additional photon emission at each period (see Fig. 24). Thus, each electron injected above threshold can generate, in principle, photons as many as there are stages (up to 75, but usually close to 30).

One of the most important consequences of a laser based on intersubband transitions is that the emission wavelength does not depend on the band gap of constituent materials, but can be tuned by tailoring the thickness of the quantum wells, as is illustrated by Fig. 25. It is thus possible to realize lasers based on quantum structures grown using mature III–V compound semiconductors such as GaAs and InP. The main factor which limits the shortest wavelength possible for a QCL is the height of the conduction band offset between the heterostructure materials, its value is currently 3.4 μm for InP-based technology and 8 μm for GaAs-based technology. On the other hand, there is no fundamental limitation (excepted the broadening of quantum levels) on the long-wavelength side. As a consequence, it has been possible to realize QCL emitting as far as in the THz-wave domain.

The critical issue of QCLs is the large amount of heat that must be dissipated in the device to achieve CW operation at room temperature. Indeed, considering that the best reported wall-plug efficiencies are of the order of a few percent and can be extrapolated to ≈10% from simulations [64], almost all the injected electrical power is converted into heat in the device. For typical 7–10 V operating voltages and threshold current of 1 W, about 10 W must thus be dissipated to prevent the active region from too much heating, which would lower the quantum efficiency and could block CW

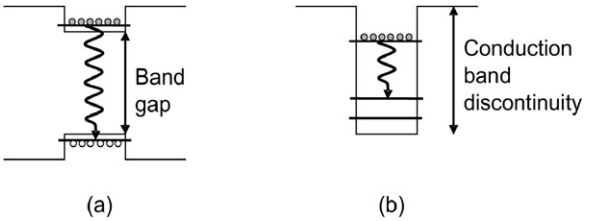

Fig. 23. Simplified band diagram illustrating the different type of optical transitions in semiconductor quantum wells. (a) interband transition: electron-hole recombination across the bandgap. (b) intersubband transition: transition between two electronic states in the conduction (valence) band, after [61].

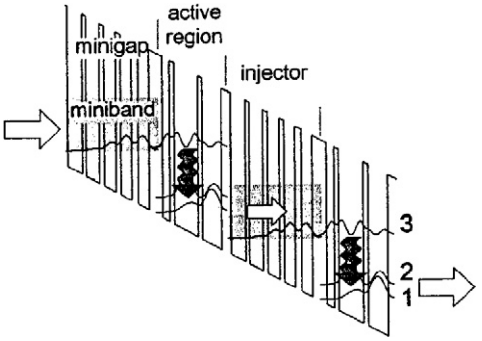

Fig. 24. Schematic conduction band diagram of two stages of a quantum cascade laser heterostructure at the threshold bias. The wavy arrow indicates the transition $3 \rightarrow 2$ responsible for the laser action. The solid curves represent the moduli squared of the relevant wavefunctions. Manifolds of closely spaced states are denoted as minibands, while the minigaps represent regions of negligible density of states, after [63].

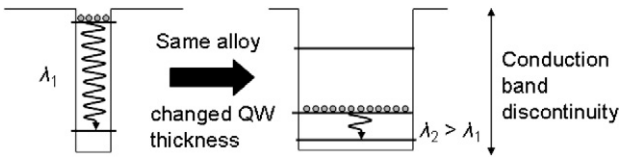

Fig. 25. Simplified band diagram illustrating that intraband transitions depend primarily on the width of the quantum well and not on the constituent materials of the heterostructure. The highest photon energy is limited by the conduction band discontinuity, while on the low energy side the limit is ultimately imposed by broadening of the quantised levels, after [61].

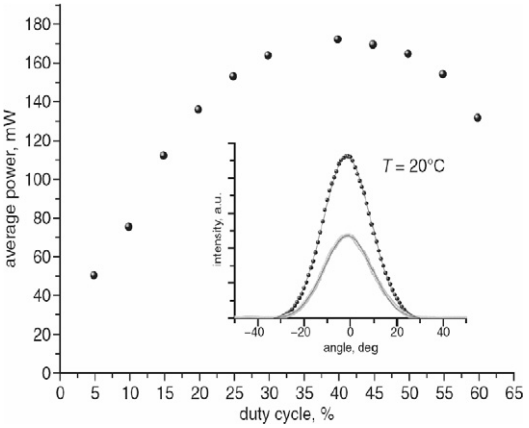

Fig. 26. Average power at room temperature against duty cycle for a quantum cascade laser emitting at 8.9 μm, after [66].

operation. If we consider the typical dimensions of the active region (for instance 5 μm × 20 μm × 2 mm, [65]), this corresponds to a huge amount of heat that must be dissipated regarding the small thermal exchange surface area. As a consequence, active cooling or modulation of the pumping current is required to improve the average output power as illustrated by Fig. 26 for a QCL emitting at 8.9 μm [66].

As shown in Fig. 27 where state-of-the-art average power is plotted as a function of wavelength [65–82], the maximal output power that has been demonstrated at room temperature is about 850 mW (at 6 μm) [69]. However, based on detailed optical and thermal simulations of QCL operation as a function of material and device parameters, output powers in the 1–3 W range in CW regime are envisioned [64]. Considering typical dimensions of the active region section of $5 \times 20\ \mu m^2$, it seems doubtful that higher average powers can be obtained form a single emitter unless sacrificing the beam quality by use of multimode waveguide structures as in high power broad area laser diodes. Indeed, current high power QCL structures already do not guaranty single-mode emission for high pumping currents. As a consequence, bistable beam steering, by far-field angles of up to $\pm 12\,^{\circ}C$ from the facet normal, has

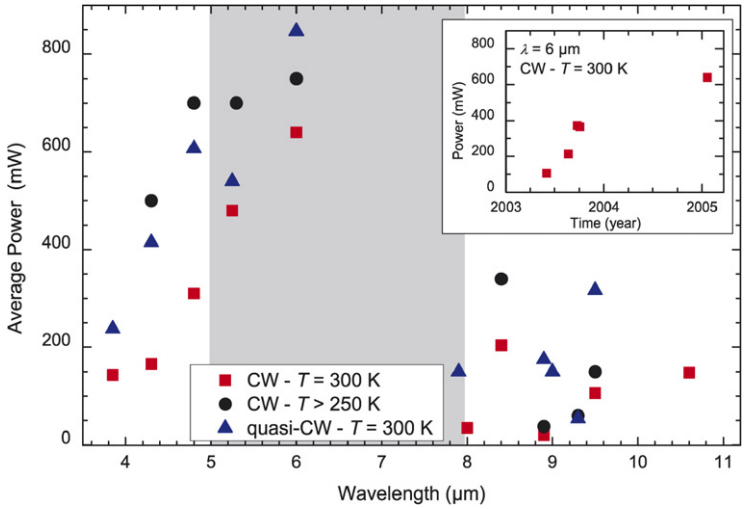

Fig. 27. Maximal power level from quantum cascade lasers demonstrated in CW and quasi-CW (pulsed) regime near room temperature and in CW regime at thermo-electric cooling temperature. The inset shows the time evolution of demonstrated CW output power at room temperature for $\lambda \approx 6$ μm. Data collected from [65–82].

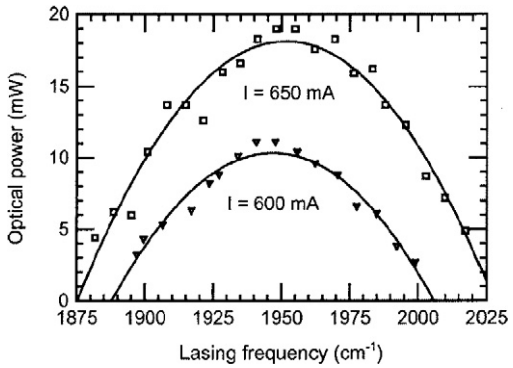

Fig. 28. Output power of a QCL external cavity laser as a function of lasing wavelength for two different values of current at $T = -30\,^{\circ}\mathrm{C}$, after [83].

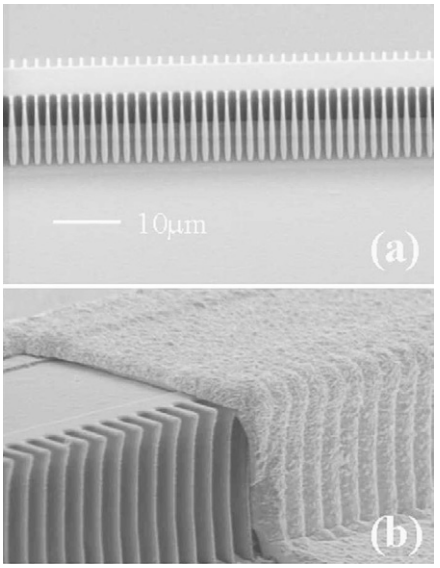

Fig. 29. (a) Scanning electron microscopy (SEM) image of lateral gratings etched in a QC laser structure using a SiO_2 mask. (b) SEM image of a QCDFB ridge with lateral gratings, after [84].

been observed as a function of current or temperature in high-power CW QCLs, which is consistent with a theory for interference and beating between the two lowest order lateral modes [75].

In the same way as other kinds of semiconductor laser, tunable and narrow linewidth QCLs have also been implemented. For instance, a tuning range of more than 260 nm around 5.15 μm with more than 10 mW over the full range has been demonstrated by use of an external cavity design as illustrated by Fig. 28 [83]. As shown in Fig. 29, distributed feedback (DFB) lasers have also been realized [84]. Recently, single-mode CW emission at several wavelengths ranging from 7.7 to 8.3 μm at a temperature of $+30\,^{\circ}\mathrm{C}$ have been obtained with DFB QCLs [81]. The frequency span, that corresponded to 8% of the center frequency was obtained by use of a bound-to-continuum active region to yield

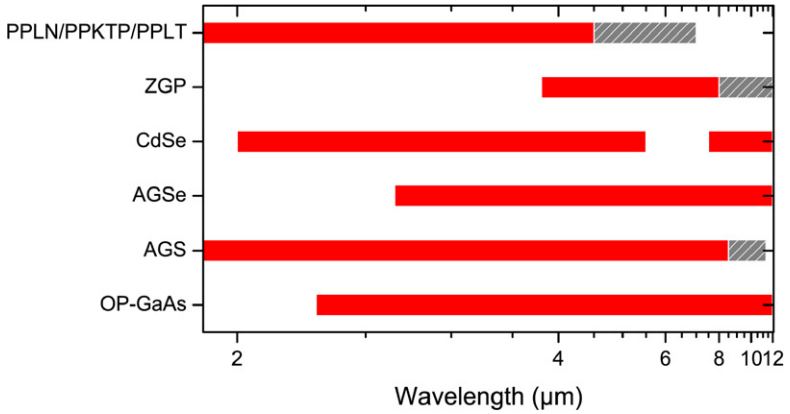

Fig. 30. Comparison of the spectral coverage of OPOs based on selected nonlinear crystals in CW and nanosecond regime. Filled areas (red) represent spectral ranges where efficient operation have been obtained while hatched areas (gray) correspond to spectral ranges where operation have been demonstrated with a reduced efficiency due to multi-phonon absorption in the considered nonlinear crystals. (For interpretation of the references to colour in this figure legend, the reader is referred to the web version of this article.)

a broad gain spectrum. A typical application of this type of DFB QCLs is in situ spectroscopic sensing, for example detection of explosives [85].

6. Optical parametric sources

Optical parametric sources (OPSs)—namely, optical parametric oscillators (OPOs), optical parametric generators (OPGs) or difference frequency generators (DFGs)—are versatile devices to generate coherent light at wavelengths where lasers perform poorly or are unavailable. Hence, OPOs downconvert a pump light of frequency ω_p into two tunable frequencies, signal frequency ω_s and idler frequency ω_i, through a nonlinear three-wave mixing process that satisfies: $\omega_p = \omega_s + \omega_i$ with $\omega_i < \omega_s$.

Since other papers are devoted to the state of the art of optical parametric sources in this special issue of C. R. Physique on infrared parametric sources, we will only give some generalities and focus on some specific points. Indeed, it is unrealistic to do justice to the huge amount of work that has been carried out on parametric sources in a short review (for example, INSPEC research database provides more than 650 references for PPLN as a keyword and more than 1900 references for KTP).

Depending on the selected nonlinear material and device architecture, OPSs can offer unique features, including:

- both continuous-wave and high-repetition-rate pulsed operations are possible with multi-watt output power;
- several 100s of mJ pulse energy can be delivered at low-repetition rates;
- a large domain of wavelengths can be covered including the whole 2–12 μm region;
- broadband as well as narrow linewidth emission spectra can be generated;
- wide tunability is achievable with a maximum infrared tuning range of 3.3–19 μm demonstrated using a GaSe OPG [86];
- rugged and compact devices can be designed.

As shown in Fig. 30, bulk and periodically poled ferroelectric oxides are suitable for implementing OPOs covering the 2–4.5 μm range. These materials—including, lithium niobate ($LiNbO_3$), potassium titanyl phosphate (KTP), potassium titanyl arsenate (KTA), or lithium tantalate ($LiTaO_3$)—are the most mature quadratic nonlinear materials and each of them can be pumped at 1 μm by use of advanced solid-state lasers. For longer wavelengths, one is required to use more uncommon materials—e.g., zinc germanium phosphide $ZnGeP_2$ (ZGP), cadmium selenide CdSe, silver thiogallate $AgGaS_2$ (AGS), silver selenogallate $AgGaSe_2$ (AGSe), or gallium arsenide GaAs—that usually also require more uncommon pump sources emitting above 2 μm.

6.1. Optical parametric sources in the 2–4.5 μm range

As explained above, OPSs in the 2–4.5 μm spectral range can be implemented using ferroelectric oxides. These nonlinear materials are suitable for direct pumping at 1 μm. Moreover, periodic poling is now well developed using electric field poling techniques [87]. Quasi-phase-matching (QPM) schemes can thus be used in periodically poled (PP) nonlinear materials with significant advantages, including.

- collinear propagation of the three interacting waves (no walk-off);
- large angular acceptance due to non-critical phase-matching scheme;
- possibility of using the largest nonlinear optical tensor element (e.g. d_{33}) which is not generally accessible with birefringent angular phase matching;
- the whole transparency range of nonlinear materials is addressable avoiding limitations on tunability imposed by the angular phase-matching condition;
- the phase-matching scheme can be engineered with multi QPM grating periods and tailored cascaded nonlinear interactions.

Thanks to these beneficial features of QPM, it is possible to implement small size OPO devices with low threshold value, high efficiency, and good beam quality. As an illustration, Fig. 31 shows a picture of a compact PPLN OPO emitting several watts of average power around 2.5 μm in nanosecond regime at high repetition rate (10 kHz) with a nearly diffraction limited beam. For longer idler wavelengths, the conversion efficiency can be improved recycling the near-IR signal wave as a pump wave for a cascaded process. Hence, using the so-called intracavity OPO–OPA scheme (also referred as OPO–DFM scheme)—whose principle is illustrated by Fig. 32 (left)—it is possible to significantly enhance the conversion efficiency toward mid-IR as proposed in [88]. Such an OPO–OPA scheme was, for instance, successfully implemented in the nanosecond regime in bulk crystals [89] as well as in PP-materials [90] where the authors demonstrated an improved conversion efficiency of 27% from 1.064 μm toward 3.80 μm (96% photon conversion efficiency) (see Fig. 32 (right)).

The low oscillation thresholds that are achievable with PP-nonlinear materials have also given rise to the development of compact and rugged narrow-linewidth OPOs that are well-suited for spectroscopy and related applications such as detection of pollutant species, remote sensing or four-wave mixing diagnostics. Hence, high-peak-power (>100 W), single-mode emission (axial and transverse), tunable in the whole 3.8–4.5 μm range can be achieved with the semimonolithic entangled-cavity doubly resonant OPO (ECOPO) scheme depicted by Fig. 33 (left) [91,92]. Moreover, thanks to its very low threshold of oscillation, the ECOPO can be pumped by a micro-laser leading to a very compact narrow linewidth tunable source, which is well suited for on board gas sensing (see Fig. 33 (right)) [93,94].

Up to now, the main limitation of PP-nonlinear materials has been the limited aperture of samples with a typical thickness of 1 mm prohibiting high pulse energy generation. Nevertheless, the recent demonstration of OPOs with large aperture PPLN samples (5×5 mm^2) emitting high-energy pulses paves the way toward high energy OPOs based on PP-materials (see Fig. 34) [95]. Indeed, the obtained energy was as high as 77 mJ for both signal (wavelength 1.83 μm) and idler (2.54 μm) waves with a 72% slope efficiency at 110 mJ pumping of a Q-switched Nd:YAG laser with a 12 ns pulse duration. Such results are thus not so far from the 430 mJ (signal + idler) pulse energy that was demonstrated near degeneracy ($\lambda \simeq 2$ μm) in a bulk $LiNbO_3$ OPO for a 950 mJ pump energy (15 ns, 10 Hz) (see Fig. 35) [96]. In this latter work, 310 mJ (respectively 250 mJ) energy and narrow linewidth of 15 GHz (respectively 1.8 GHz) were also demonstrated replacing a cavity mirror by a Littrow-mounted grating (respectively a Littrow-mounted grating and an additional solid étalon). DFG between signal and idler was then carry out in several mid-IR nonlinear crystals to generate tunable radiation in the 6–19 μm range with up to 10 mJ pulse energy at 10 μm.

Linewidth narrowing has also been recently demonstrated in a configuration with a spectrally narrowed master oscillator followed by a 5 mm × 5 mm large aperture PPLN power amplifier, where the authors have achieved an output pulse energy of 52 mJ with a spectral bandwidth of less than 2 nm at the degeneracy point [97]. In this work, spectral narrowing of the master oscillator was carried out by use of a solid étalon and a Littrow-mounted grating as well. In a very recent work, a source based on a similar design has been used as a pump source for DFG in a $ZnGeP_2$ crystal [98]. Narrow linewidth sources near degeneracy are indeed very useful to pump (type I) ZGP OPOs where the pump spectral acceptance is very limited. A promising technique to realize such 2 μm narrow-linewidth pump sources avoiding complicated OPO resonator schemes is to replace the conventional output coupler by a volume

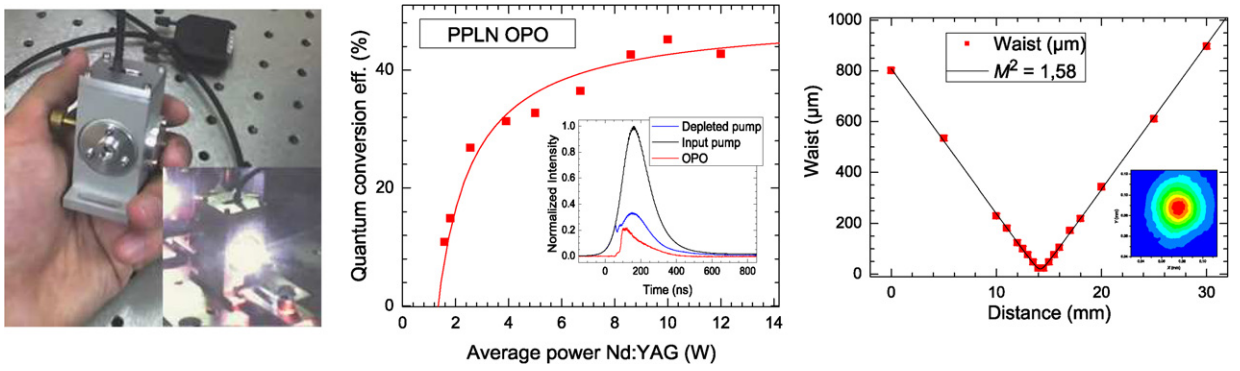

Fig. 31. Picture of a compact PPLN OPO emitting around 2.5 μm (insert: the OPO under operation) (left), quantum efficiency as a function of the pump power (insert: temporal profiles of incident pump, depleted pump and emitted idler pulses) (middle), and corresponding beam quality (right).

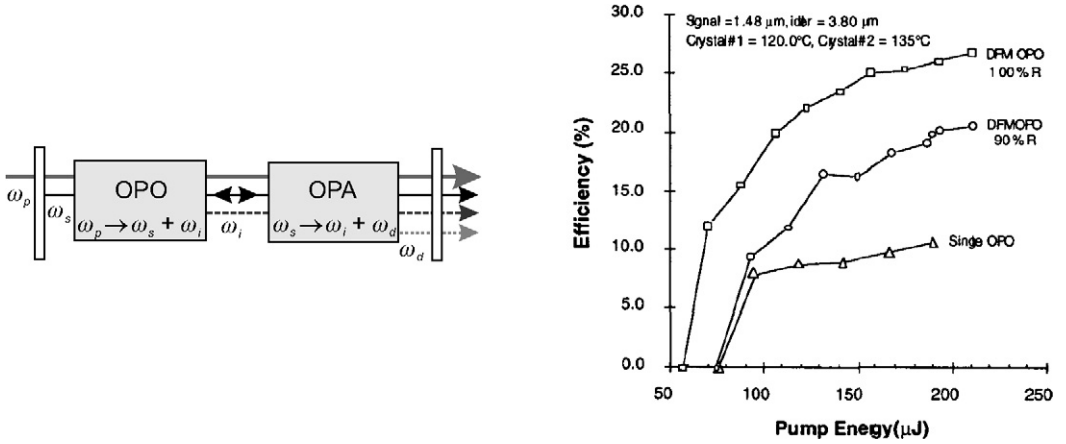

Fig. 32. Schematic diagram of the OPO–OPA scheme (the intracavity OPA crystal is designed to phase match the signal and idler waves to produce a difference frequency photon and an additional idler photon) (left), conversion efficiency of a PPLN OPO–OPA device as a function of the pump power (right), after [90].

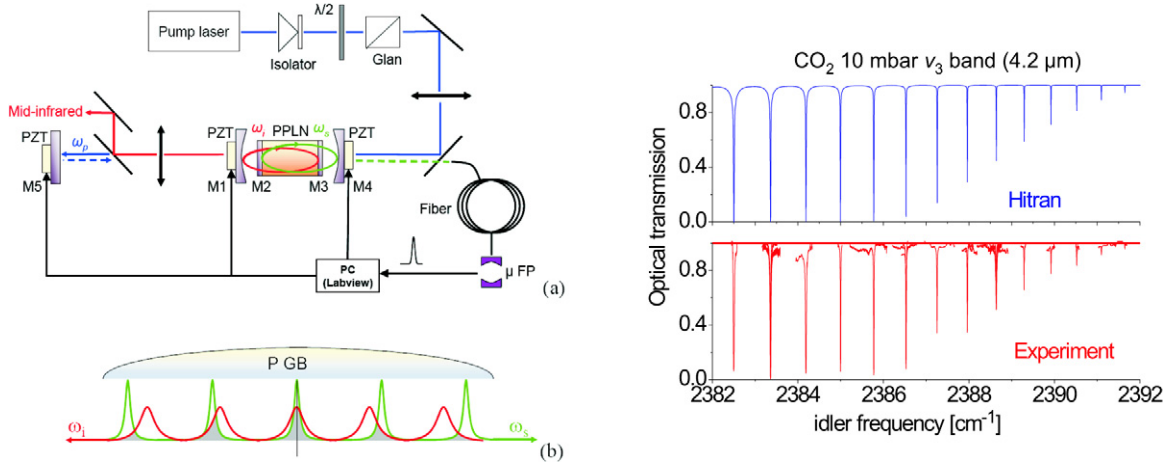

Fig. 33. Schematic of the ECOPO setup with a partial pump beam reflection (left, a); ECOPO signal and idler mode overlap (PGB: Parametric Gain Bandwidth), a perfect coincidence is shown at the central position whereas other coincidences are imperfect, leading to single-frequency output (left, b), after [94]. Theoretical (top) and experimental (bottom) spectra of CO_2 measured by use of the ECOPO at a 10 mbar pressure (right).

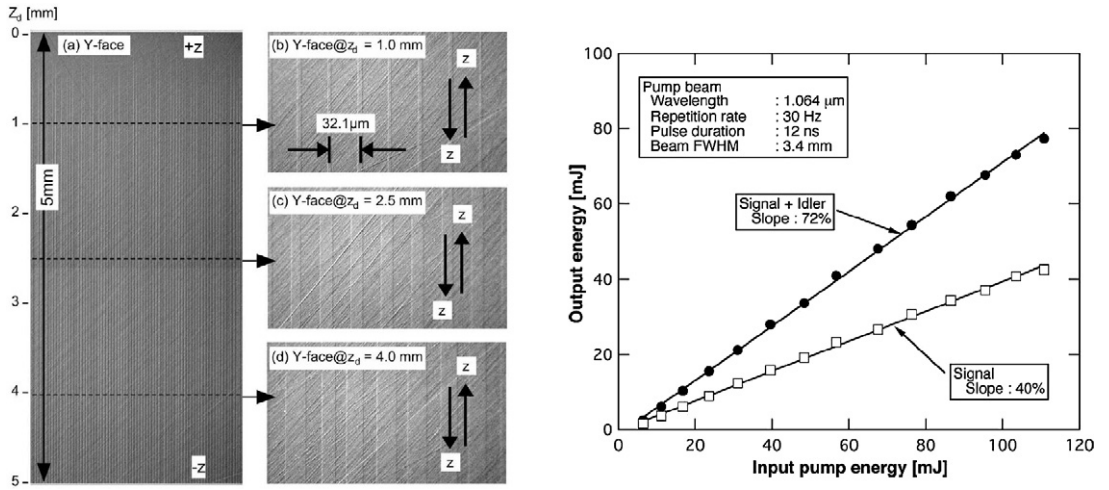

Fig. 34. Photographs of etched surface of a large aperture (5×5 mm^2) PPLN sample (left) and OPO output energy dependence on input pump energy (right), after [95].

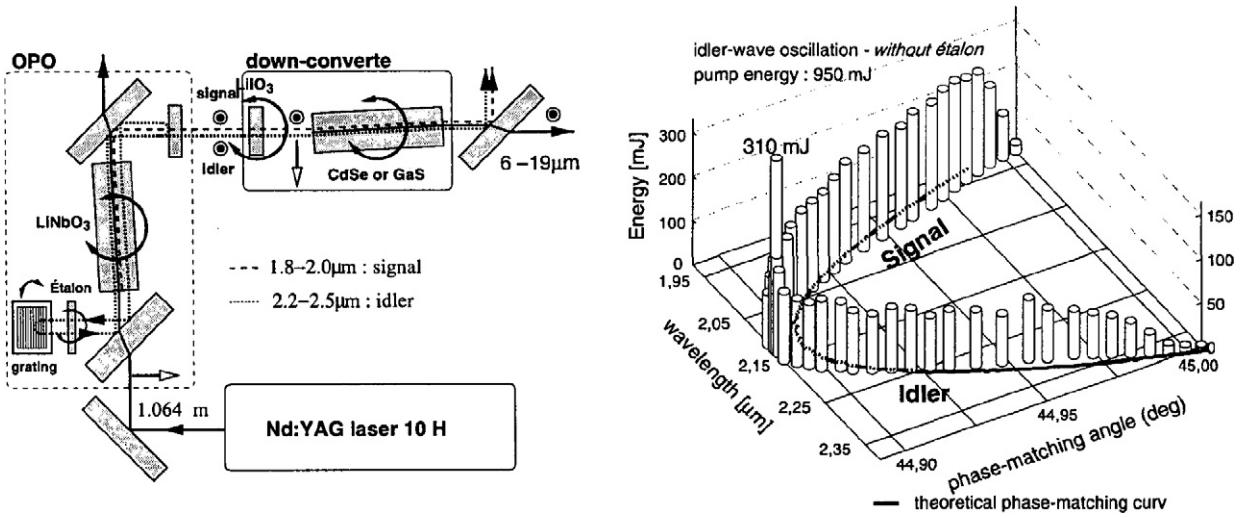

Fig. 35. Schematic diagram of a high-energy $LiNbO_3$ OPO followed by a DFG stage (left) and OPO output energy as a function of the output wavelengths without intracavity étalon, for a pump energy of 950 mJ (right), after [96].

Bragg grating. This scheme was for instance demonstrated in a PPKTP OPO where the narrowed 2008 nm radiation was subsequently used for pumping the ZGP OPO (see Fig. 36) [99].

Optical parametric amplification is very convenient to boost the energy while keeping the narrow linewidth emission. However, it can lead to strong spatial distortions of the amplified beam profile because of pump reconversion. In order to maintain a good beam quality, the amplifier stage has to be designed in such a manner that the back conversion effect remains limited. As reported in [100], one can reduce this detrimental effect by using multi-crystal OPA configuration with a spectral filtering inserted between successive crystals (see Fig. 37 (right)). In such conditions, one can separate the signal from the idler radiation (or vice-versa) before passing through the next amplifier, reducing so the back conversion effect. Following this approach, it is possible to achieve a high optical conversion efficiency (close to 30%) while maintaining a good beam quality (see Fig. 37 (left)).

6.2. Optical parametric sources in the 4.5–12 µm range

Above 4.5 µm, standard oxide nonlinear materials ($LiNbO_3$, KTP, KTA, ...) exhibit strong bulk absorptions and are thus unsuitable. As a result, it is required to implement parametric sources based on less developed materials whose

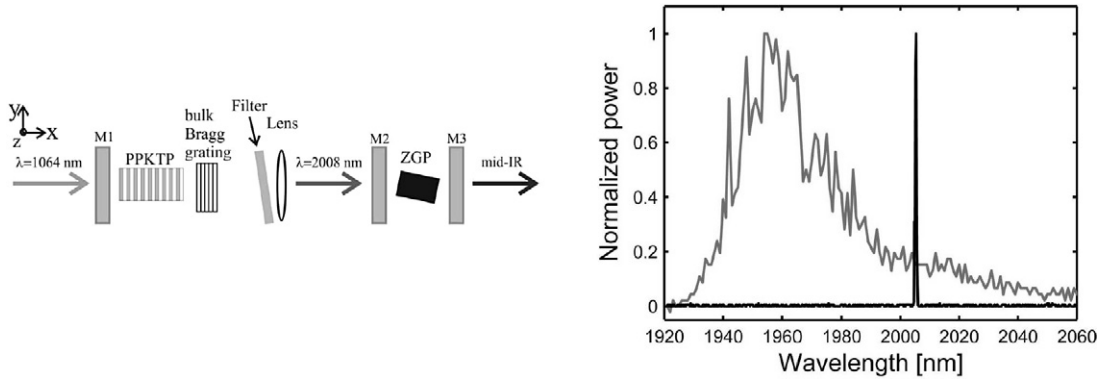

Fig. 36. Schematic diagram of a tandem OPO setup including a PPKT OPO (whose linewidth is narrowed by use of a volume Bragg grating) and a ZGP OPO (left) and emitted signal spectra from the PPKTP OPO with a conventional mirror (gray curve) and a volume Bragg grating as an output coupler (black curve) (right), after [99].

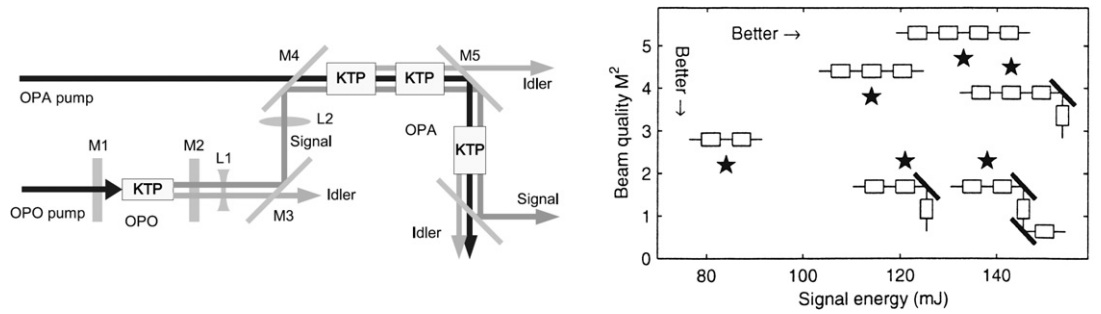

Fig. 37. Schematic diagram of a KTP MOPA system for conversion from 1.064 μm to 2.1 μm (left). Signal energy and estimated beam quality (M^2) for various OPA configurations with a pump energy of 500 mJ (the sketches indicate the number of OPA crystals and idler output coupler and the stars are the actual data points) (right), after [100].

optical quality is less controlled and that also usually require pump sources emitting above 2 μm. As shown in Fig. 38, where published output powers and energies are reported as a function of emission wavelength [44,96,100–104,106, 107], the best performance has been obtained with ZGP-based OPSs. Indeed, up to 30 W average power have been demonstrated at high repetition rate as well as 30 mJ (signal + idler) pulse energy at low repetition rate. However, because of ZGP bulk absorption above 8 μm, this crystal is not relevant to produce efficient tunable emission in the 8–12 μm spectral region as illustrated by Fig. 39 from [108] showing the output energy of a singly resonant angle-tuned ZGP OPO pumped by 100-ns erbium laser pulses at 2.93 μm as a function the emitted wavelength.

Currently, the best performance in the 8–12 μm has been obtained with CdSe-based OPSs with up to 10 mJ pulse energy obtained at 10 Hz repetition rate by DFG from signal and idler of a high-energy $LiNbO_3$ OPO (see Fig. 35 (left)) [96]. CdSe OPOs have been implemented emitting millijoule level pulse energies in almost the whole 8–12 μm range using, for instance, a Cr,Er:YSGG laser emitting at 2.79 μm (OPO emission: 8.5–12.3 μm, see Fig. 40) [109] or a KTA OPO tunable between 2.99 and 3.45 μm (OPO emission: 8.31–10.58 μm) [110] as pump sources.

More recently, the first CdSe-based device emitting more than 1 W of average power has been reported [44]. It consists in a Cr:ZnSe laser-pumped, intracavity CdSe OPO with signal and idler tunable from 3.2 to 3.8 μm and 8.2 to 8.5 μm respectively and output power of 2 W (signal + idler) at 5 kHz repetition rate. The output wavelength was pump tuned by use of an intracavity acousto-optical filter with no moving mechanical component. Tunability was demonstrated in the 8.2–8.8 μm range with a maximal idler power of 1.1 W at 8.2 μm (see Fig. 41).

In addition to the birefringent phase-matched materials, orientation patterned GaAs (OP-GaAs) is currently emerging as a promising QPM material for OPSs emitting above 4.5 μm. The first OP-GaAs based OPO has been recently demonstrated emitting 3 μJ at 7.9 μm with a 5.78–9.14 μm tuning range [111]. Since then, direct pumping by a Tm,Ho:YLF laser emitting at 2.05 μm has been implemented with an output power of 442 mW (signal at 3.5 μm +

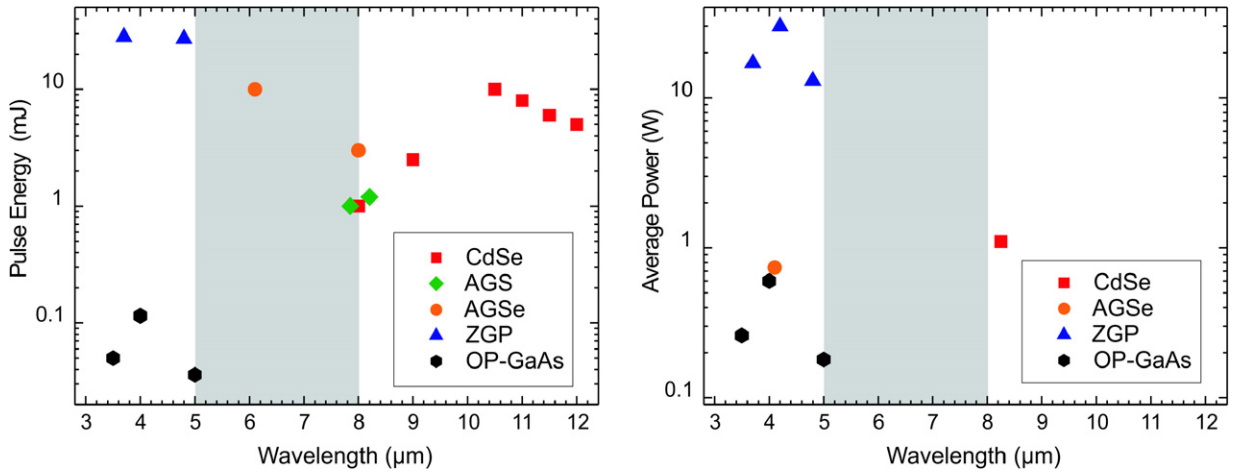

Fig. 38. Best reported performances of parametric sources based on mid-IR nonlinear crystals suitable for emission above 4.5 μm in nanosecond regime: pulse energy (left) and average power at high repetition rate (right). Data collected from [44,96,100–104,106,107].

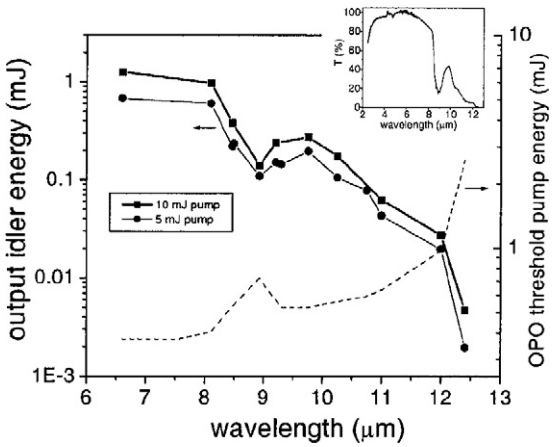

Fig. 39. Output energy of a ZGP OPO as a function of the idler wavelength for two pump energies: 5 and 10 mJ. Dashed curve, the OPO pump threshold dependence. Inset, transmission spectrum of the antireflection-coated $L = 2$ cm ZGP crystal, after [108].

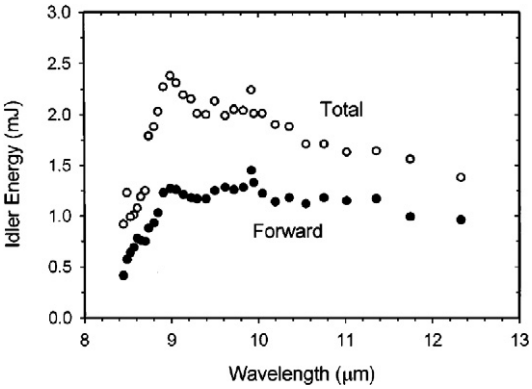

Fig. 40. Total and forward idler output energies from a CdSe OPO with a 2.79-μm pump energy of 22–25 mJ, after [109].

idler at 4.98 μm) from 2.6 W of pump power at 10 kHz rep. rate [105]. More recently, up to 0.6 W has been obtained with a 2-μm pumped OP-GaAs OPO [106].

OP-GaAs is also an interesting material to realize a DFG narrow linewidth CW tunable source for in situ spectroscopic measurement in the long-wave IR. For example, as reported in [112], the outputs from two tunable, external cavity diode lasers covering the 1.3 μm and 1.5 μm telecom bands were amplified and then mixed in an OP-GaAs crystal (see Fig. 42 (left)), producing several microwatts of tunable radiation in the 7–9 μm region (see Fig. 42 (right)). When combined with ultra-sensitive absorption methods such as cavity ring-down spectroscopy, OP-GaAs could thus be a valuable material for use in detection of large molecular weight, low vapor pressure molecules.

7. Discussion

Fig. 43 depicts the spectral coverage of the technologies presented in this review. As one can see, two sub-spectral ranges can be considered:

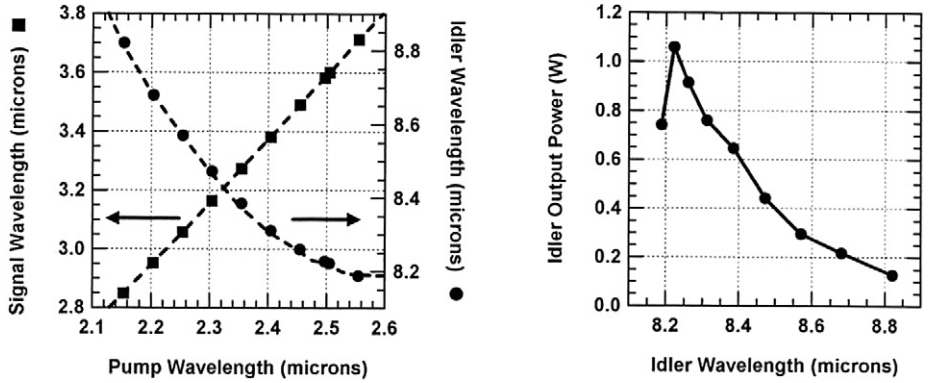

Fig. 41. Signal (squares—left axis) and idler (circles—right axis) wavelengths as a function of Cr:ZnSe pump wavelength (left). Idler power as a function of idler wavelength (right), after [44].

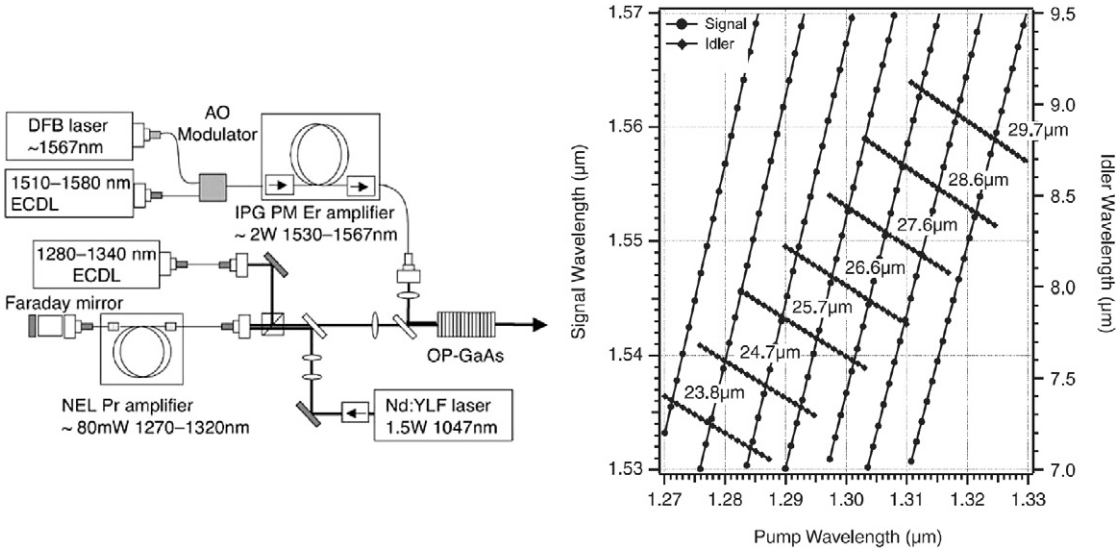

Fig. 42. Simplified schematic of an OP-GaAs based DFG system (the praseodymium amplifier is a double-pass configuration with the input and output on the same end) (left) and tuning ranges achievable with a multi-grating OP-GaAs crystal and tunable telecom sources in the 1550 nm and 1300 nm bands (right), after [112].

– 2–3 μm range that includes the emission spectra of most of the technologies;
– 3–12 μm range where the choice is restricted to quantum cascade lasers and parametric sources.

The discussion is thus organized with respect to these two sub-ranges in the context of several selected applications.

7.1. Comparative study in the 2–3 μm range

As shown in Table 2, where some key-features of sources emitting in the 2–3 μm spectral range are summarized, the technologies considered display complementary characteristics. The proper choice is thus determined by the relevance of these technologies in the context of each considered application. Our findings are discussed for the following selected applications:

– In situ chemical sensing,
– LIDAR and nonlinear spectroscopy,
– Laser and OPO pumping,
– Surgery.

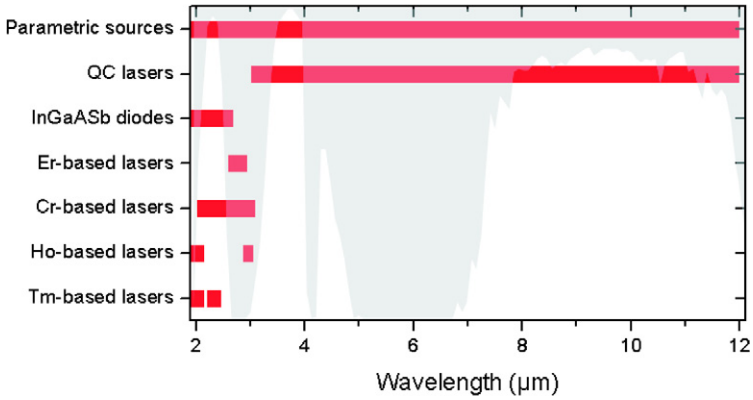

Fig. 43. Spectral coverage of the infrared sources considered in this review.

Table 2
Summary of the main features and best reported performances of considered sources in the 2–3 μm spectral range

Technology	Laser diodes	Rare-earth lasers	Cr:ZnSe lasers	Parametric sources
Regime	CW or quasi-CW	CW as well as pulsed	CW or pulsed (with pulsed pump)	*Pulsed* (with pulsed pump) or CW
Average power	>1 W/emitter	>100 W	∼2 W (CW) ∼30 W (pulsed)	∼50 W
Energy	–	>1 J (Ho)	∼4 mJ	∼400 mJ
Tunability	200 nm with low power	300 nm (Tm)	1200 nm	Full range
Pumping	Electrical (or optical)	Diode or laser	Diode or laser (maybe electrical)	Laser

Many other applications could have been considered. Nevertheless, the needs covered by the four above mentioned applications can be supposed representative of more general requirements. In this way, the choice of the proper laser source can be carry out according to the same methodology as for the four considered applications.

7.1.1. In situ chemical sensing

This class of applications includes absorption spectroscopy, cavity ringdown spectroscopy (CRDS) and related techniques. These applications usually require compact light emitters with narrow linewidth while output power is not a critical issue. Moreover, CW or pulsed operations may be suitable.

If the sensor is dedicated to a reduced number of chemical species, resulting in a reduced required tunability, the use of tunable laser diodes (DFB, ECL) seems to be the most suitable choice to implement an integrated device with a limited cost.

On the other hand, versatile devices with broad tuning ranges should be implemented with parametric sources or Cr:ZnSe lasers. Such sensors would be obviously more expensive than laser-diode-based ones. Nevertheless, one should note that very compact device are expected in the near future thanks to the emergence of micro-laser pumped tunable OPOs.

7.1.2. LIDAR and nonlinear spectroscopy

Mid-IR LIDAR are useful for atmosphere remote sensing applications such as greenhouse or pollutant gases monitoring, atmospheric profiling, terrain and city mapping, canopy and vegetation mapping, etc. Pulsed operation is thus required to achieve range resolved measurements.

In situ optical sensing for combustion and hypersonic flows studies also involve pulsed sources since such metrology techniques rely on nonlinear spectroscopy, including four-wave mixing or coherent anti-Stokes Raman scattering, that requires high peak intensity input beams to generate a measurable signal.

Most of the requirement can be fulfilled with OPOs or a Cr:ZnSe laser that provide wide tunability and pulsed operation in the whole 2–3 μm range. OPOs would be preferred for pulse energy larger than several millijoules.

If even much high pulse energy is required, Tm–Ho-based lasers provide unique features at the price of a limited tunability around 2 μm. Tm-based sources can also be very interesting thanks to their high wall-plug efficiency.

7.1.3. Laser and OPO pumping

As presented in this review, optical pumping of several of the considered infrared laser sources can be achieved with sources emitting in the 1.8–3 μm range, as summarized as it follows:

– Cr:ZnSe laser can be efficiently pumped by high-power laser diodes for CW operation or Tm-based lasers for CW as well as pulsed operation (OPOs can also be used as pump sources with usually a smaller efficiency);
– Ho-based laser can be directly pumped at 1.9 μm by Tm-based lasers or Tm–Ho co-doping can be used for laser diode pumping;
– Parametric sources can be pumped by all of the considered sources (more straightforwardly with pulsed sources for OPO pumping), the proper choice depends on the nonlinear crystal (absorption, phase-matching conditions, ...).

7.1.4. Surgery

Er-based and Ho-based lasers emitting at 3 μm are the most relevant for surgical applications since the related laser emission coincides with O–H vibration in water and is thus strongly absorbed by biological tissues.

7.2. Comparative study in the 3–12 μm range

As shown by Fig. 43, only two options remains in the 3–12 μm spectral range: parametric sources and quantum cascade lasers. Because of this limited choice, we include CO_2 laser in addition to these two solid-state technologies in Table 3 that summarized the same key-features as Table 2, in the 3–12 μm spectral range.

In the same manner as in Section 7.1, the available technologies are discussed in the context of the following applications whose needs are supposed to be representative of more general requirements:

– In situ chemical sensing,
– LIDAR and nonlinear spectroscopy,
– Military applications,
– Cutting and welding.

7.2.1. In situ chemical sensing

As explained in Section 7.1.1, the related applications require compact light emitter with narrow linewidth and tunable emission while output power is not a critical issue. In this context, quantum cascade lasers appear as the most promising sources for application requiring a limited tunability. Nevertheless, for wavelength bellow 4.5 μm, very compact OPO sources can also be competitive compared to external cavity QCL. Moreover, parametric sources remains a good option if a broader tuning range is required.

7.2.2. LIDAR and nonlinear spectroscopy

Since this class of applications require optical sources operating in pulsed regime (see Section 7.1.2), parametric sources are the most relevant choice. However, the implementation of such sources is still challenging above 8 μm because of laser pump and nonlinear material issues.

Table 3
Summary of the main features and best reported performances of considered sources in the 3–12 μm spectral range

Technology	CO_2 lasers	Quantum cascade lasers	Parametric sources
Regime	CW or quasi-CW	CW or quasi-CW	*Pulsed* (with pulsed pump)or CW
Average power	∼400 W (compact systems)	∼1 W ($\lambda > 4.5$ μm)	∼30 W ∼1 W ($\lambda > 8$ μm, pump limited)
Energy	–	–	∼30 mJ ∼10 mJ ($\lambda > 8$ μm)
Tunability	Discrete 9.15–9.83 μm + 10.09–10.93 μm	∼400 nm (low power) ∼2000 nm (very low power)	∼8600 nm (OPO) ∼15700 nm (OPG)
Pumping	Electrical	Electrical	Laser

7.2.3. Military applications

Quantum cascade lasers are promising military sources for applications where CW emission with moderate average power and tunability is acceptable. For other applications requiring high peak and/or average power with broad tunability, OPOs are still the most relevant technology. As for LIDAR and nonlinear spectroscopy, one should mention that the development of reliable OPOs emitting above 8 μm is still challenging.

7.2.4. Cutting and welding

The high average power required by this kind of applications is not currently conceivable with OPOs or quantum cascade lasers. CO_2 laser thus remains unbeatable in this spectral range for this class of applications.

8. Conclusions

In this review article, we have briefly presented the main properties and best reported performances of some of the most advanced coherent source technologies emitting in the 2–12 μm spectral range. Their relative capabilities have been discussed in the context of several applications, showing that the reported technologies are complementary and relevant depending on the considered application. Hence, similarly to the visible/near-IR range where several technologies coexist, each of the considered technology can be found as the most relevant one for at least a specific class of applications. Another important observation following this review is that only two solid-state technologies can currently provide efficient emission at wavelengths longer than 3 μm; namely, parametric sources and quantum cascade lasers.

Acknowledgements

The author is grateful to his colleagues Myriam Raybaut and Michel Lefebvre for their careful reading and valuable suggestions.

References

[1] I.T. Sorokina, K.L. Vodopyanov (Eds.), Solid-State Mid-Infrared Sources, Topics in Applied Physics, vol. 89, Springer, Berlin, Heidelberg, 2003.
[2] J. Wu, Z. Yao, J. Zong, S. Jiang, Highly efficient high-power thulium-doped germanate glass fiber laser, Opt. Lett. 32 (2007) 638–640.
[3] D.G. Lancaster, A. Sabella, A. Hemming, S. Bennetts, S.D. Jackson, Power-scalable thulium and holmium fibre lasers pumped by 793 nm diode lasers, in: Advanced Solid-State Photonics 2007, The Optical Society of America, Washington, 2007, Technical Digest, WE5.
[4] IPG Photonics, http://www.ipgphotonics.com/.
[5] K.S. Lai, P.B. Phua, R.F. Wu, Y.L. Lim, E. Lau, S.W. Toh, B.T. Toh, A. Chng, 120-W continuous-wave diode-pumped Tm:YAG laser, Opt. Lett. 25 (2000) 1591–1593.
[6] A. Dergachev, K. Wall, P.F. Moulton, A CW side-pumped Tm:YLF laser, in: M. Ferman, L. Marshall (Eds.), Trends in Optics and Photonics, in: Advanced Solid-State Lasers, vol. 68, Optical Society of America, 2002, pp. 343–346.
[7] A.C. Sullivan, A. Zakel, G.J. Wagner, D. Gwin, B. Tiemann, R.C. Stoneman, A.I.R. Malm, High power Q-switched Tm:YALO lasers, in: G.J. Quarles (Ed.), Trends in Optics and Photonics, in: Advanced Solid-State Photonics, vol. 94, Optical Society of America, 2004, pp. 329–332.
[8] M. Eichhorn, Development of a high-pulse-energy Q-switched Tm-doped double-clad fluoride fiber laser and its application to the pumping of mid-IR lasers, Opt. Lett. 32 (2007) 1056–1058.
[9] N. Coluccelli, D. Gatti, G. Galzerano, F. Cornacchia, D. Parisi, A. Toncelli, M. Tonelli, P. Laporta, Tunability range of 245 nm in a diode-pumped Tm:BaY_2F_8 laser at 1.9 μm: a theoretical and experimental investigation, Appl. Phys. B 85 (2006) 553–555.
[10] J.F. Pinto, L. Esterowitz, G.H. Rosenblatt, Tm^{3+}:YLF laser continuously tunable between 2.20 and 2.46 μm, Opt. Lett. 19 (1994) 883–885.
[11] R.C. Stoneman, L. Esterowitz, Efficient, broadly tunable, laser-pumped Tm:YAG and Tm:YSGG CW lasers, Opt. Lett. 15 (1990) 486–488.
[12] R.C. Stoneman, L. Esterowitz, Efficient 1.94 μm Tm:YALO laser, IEEE J. Sel. Topics Quantum Electron. 1 (1995) 78–80.
[13] L. Fornasiero, N. Berner, B.-M. Dicks, E. Mix, V. Peters, K. Petermann, G. Hubert, Broadly tunable laser emission from Tm:Y_2O_3 and Tm:Sc_2O_3 at 2 μm, in: M. Fejer, H. Injeyan, U. Keller (Eds.), Trends in Optics and Photonics, in: Advanced Solid-State Lasers, vol. 26, Optical Society of America, 1999, pp. 450–453.
[14] W.A. Clarkson, N.P. Barnes, P.W. Turner, J. Nilsson, D.C. Hanna, High-power cladding-pumped Tm-doped silica fiber laser with wavelength tuning from 1860 to 2090 nm, Opt. Lett. 27 (2002) 1989–1991.
[15] E. Sorokin, A.N. Alpatiev, I.T. Sorokina, A.I. Zagumennyi, I.A. Shcherbakov, Tunable efficient continuous-wave room-temperature Tm^{3+}:$GdVO_4$ laser, in: M. Ferman, L. Marshall (Eds.), Trends in Optics and Photonics, in: Advanced Solid-State Lasers, vol. 68, Optical Society of America, 2002, pp. 347–350.
[16] D.Y. Shen, J.K. Sahu, W.A. Clarkson, J. Nilsson, D.C. Hanna, High-power widely tunable Tm:fibre lasers pumped by an Er, Yb co-doped fibre laser at 1.6 μm, Opt. Express 14 (2006) 6084–6090.

[17] B. Jean, T. Bende, Mid-IR laser application in medicine, in: I.T. Sorokina, K.L. Vodopyanov (Eds.), Solid-State Mid-Infrared Sources, in: Topics in Applied Physics, vol. 89, Springer, Berlin Heidelberg, 2003, pp. 511–544.
[18] J. Yu, B.C. Trieu, E.A. Modlin, U.N. Singh, M.J. Kavaya, S. Chen, Y. Bai, P.J. Petzar, M. Petros, 1 J/pulse Q-switched 2 μm solid-state laser, Opt. Lett. 31 (2006) 462–464.
[19] T.Y. Fan, G. Huber, R.L. Byer, P. Mitzscherlich, Spectroscopy and diode laser-pumped operation of Tm,Ho:YAG, IEEE J. Quantum Electron. 24 (1988) 924–933.
[20] P.A. Budni, L.A. Pomeranz, M.L. Lemons, C.A. Miller, J.R. Mosto, E.P. Chicklis, Efficient mid-infrared laser using 1.9 μm-pumped Ho:YAG and $ZnGeP_2$ optical parametric oscillators, J. Opt. Soc. Am. B 17 (2000) 723–728.
[21] E. Lippert, S. Nicolas, G. Arisholm, K. Stenersen, G. Rustad, Midinfrared laser source with high power and beam quality, Appl. Opt. 45 (2006) 3839–3845.
[22] C.D. Nabors, J. Ochoa, T.Y. Fan, A. Sanchez, H.K. Choi, G.W. Tumer, Ho:YAG laser pumped by 1.9 μm diode lasers, IEEE J. Quantum Electron. 31 (1995) 1603–1605.
[23] A. Dergachev, P. Moulton, T.E. Drake, High power, high energy Ho:YLF laser pumped with Tm:fiber laser, in: C. Denman, I.T. Sorokina (Eds.), Trends in Optics and Photonics, in: Advanced Solid-State Photonics, vol. 98, Optical Society of America, 2005, pp. 608–612.
[24] Y.D. Zavartzev, V.V. Osiko, S.G. Semenkov, P.A. Studenikin, A.F. Umyskov, Cascade laser oscillation due to Ho^{3+} ions in a (Cr,Yb,Ho):YSGG yttrium–scandium–gallium garnet crystal, Sov. J. Quantum Electron. 23 (1993) 312–316; transl. from: Kvan. Elektron. 20 (1993) 366–370.
[25] S.D. Jackson, Single-transverse-mode 2.5-W holmium-doped fluoride fiber laser operating at 2.86 μm, Opt. Lett. 29 (2004) 334–336.
[26] A. Diening, S. Kück, Spectroscopy and diode-pumped laser oscillation of Yb^{3+}, Ho^{3+}-doped yttrium scandium gallium garnet, J. Appl. Phys. 87 (2000) 4063–4068.
[27] X. Zhu, R. Jain, 10-W-level diode-pumped compact 2.78 μm ZBLAN fiber laser, Opt. Lett. 32 (2007) 26–28.
[28] A. Dergachev, P. Moulton, Tunable CW Er:YLF diode-pumped laser, in: Advanced Solid-State Photonics, Optical Society of America, 2003, pp. 5–7, Technical Digest.
[29] A. Zajac, M. Skorczakowski, J. Swiderski, P. Nyga, Electrooptically Q-switched mid-infrared Er:YAG laser for medical applications, Opt. Express 12 (2004) 5125–5130.
[30] H. Voss, F. Massmann, Diode-pumped Q-switched erbium lasers with short pulse duration, in: R.C. Pollock, W.R. Bosenberg (Eds.), Trends in Optics and Photonics, in: Advanced Solid-State Lasers, vol. 10, Optical Society of America, 1997, pp. 217–221.
[31] L.D. Deloach, R.H. Page, G.D. Wilke, S.A. Payne, W.F. Krupke, Transition metal-doped zinc chalcogenides: spectroscopy and laser demonstration of a new class of gain media, IEEE J. Quantum Electron. 32 (1996) 885–895.
[32] I.T. Sorokina, Cr^{2+}-doped II–VI materials for lasers and nonlinear optics, Opt. Mat. 26 (2004) 395–412.
[33] E. Sorokin, S. Naumov, I.T. Sorokina, Ultrabroadband infrared solide-state lasers, IEEE J. Sel. Topics Quantum Electron. 11 (2005) 690–712.
[34] A.V. Podlipensky, V.G. Shcherbitsky, N.V. Kuleshov, V.I. Levchenko, V.N. Yakimovich, M. Mond, E. Heumann, G. Huber, H. Kretschmann, S. Kück, Efficient laser operation and continuous-wave diode pumping of Cr^{2+}:ZnSe single crystals, Appl. Phys. B 72 (2001) 253–255.
[35] S.B. Mirov, V.V. Fedorov, K. Graham, I.S. Moskalev, V.V. Badikov, V. Panyutin, Erbium fiber laser-pumped continuous-wave microchip Cr^{2+}:ZnS and Cr^{2+}:ZnSe lasers, Opt. Let. 27 (2002) 909–911.
[36] M. Mond, D. Albrecht, E. Heumann, G. Huber, S. Kück, V.I. Levchenko, V.N. Yakimovich, V.G. Shcherbitsky, V.E. Kisel, N.V. Kuleshov, M. Rattunde, J. Schmitz, R. Kiefer, J. Wagner, 1.9 μm and 2.0 μm laser diode pumping of Cr^{2+}:ZnSe and Cr^{2+}:CdMnTe, Opt. Let. 27 (2002) 1034–1036.
[37] U. Demirbas, A. Sennaroglu, Intracavity-pumped Cr^{2+}:ZnSe laser with ultrabroad tuning range between 1880 and 3100 nm, Opt. Lett. 31 (2006) 2293–2295.
[38] I.T. Sorokina, E. Sorokin, Chirped-mirror dispersion controlled femtosecond Cr:ZnSe laser, in: Advanced Solid-State Photonics, Optical Society of America, 2007, OSA Technical Digest Series (CD), paper WA7.
[39] G.J. Wagner, T.J. Carrig, Power scaling of Cr^{2+}:ZnSe lasers, in: C. Marshall (Ed.), Trends in Optics and Photonics, in: Advanced Solid-State Lasers, vol. 50, Optical Society of America, 2001, pp. 506–510.
[40] A. Zakel, G.J. Wagner, A.C. Sullivan, J.F. Wenzel, W.J. Alford, T.J. Carrig, High-brightness, rapidly-tunable Cr:ZnSe lasers, in: C. Denman, I.T. Sorokina (Eds.), Trends in Optics and Photonics, in: Advanced Solid-State Photonics, vol. 98, Optical Society of America, 2005, pp. 723–727.
[41] T.J. Carrig, A.K. Hankla, G.J. Wagner, C.B. Rawle, I.T. McKinnie, Tunable infrared laser sources for DIAL, in: G.W. Kamerman (Ed.), Laser Radar Technology and Applications VII, in: Proc. SPIE, vol. 4723, 2002, pp. 147–155.
[42] E. Sorokin, I.T. Sorokina, C. Fischer, M.W. Sigrist, Widely tunable Cr^{2+}:ZnSe laser source for trace-gas sensing, in: C. Denman, I.T. Sorokina (Eds.), Trends in Optics and Photonics, in: Advanced Solid-State Photonics, vol. 98, Optical Society of America, 2005, pp. 826–830.
[43] A. Zakel, G.J. Wagner, W.J. Alford, T.J. Carrig, High-power, rapidly-tunable $ZnGeP_2$ intracavity optical parametric oscillator, in: Conference on Lasers and Electro-Optics, Optical Society of America, 2005, Technical Digest, paper CThY5.
[44] A. Zakel, G.J. Wagner, W.J. Alford, T.J. Carrig, High-power, rapidly tunable dual band CdSe optical parametric oscillator, in: C. Denman, I.T. Sorokina (Eds.), Trends in Optics and Photonics, in: Advanced Solid-State Photonics, vol. 98, Optical Society of America, 2005, pp. 433–437.
[45] V.V. Fedorov, I. Moskalev, L. Luke, A. Gallian, S.B. Mirov, Mid-infrared electroluminescence of Cr^{2+} ions in ZnSe crystals, in: Advanced Solid-State Photonics, Optical Society of America, 2006, Technical Digest, WB21.
[46] J. Jaeck, R. Haidar, E. Rosencher, M. Caes, M. Tauvy, S. Collin, N. Bardou, J.L. Pelouard, F. Pardo, P. Lemasson, Room-temperature electroluminescence in the mid-infrared (2–3 μm) from bulk chromium-doped ZnSe, Opt. Lett. 31 (2006) 3051–3053.

[47] V.V. Fedorov, S.B. Mirov, A. Gallian, D.V. Badikov, M.P. Frolov, Y.V. Korostelin, V.I. Kozlovsky, A.I. Landman, Y.P. Podmar'kov, V.A. Akimov, A.A. Voronov, 3.77–5.05 μm tunable solid-state lasers on Fe^{2+}-doped ZnSe crystals operating low and room temperatures, IEEE J. Quantum Electron. 42 (2006) 907–917.
[48] A. Joullié, P. Christol, A.N. Baranov, A. Vicet, Mid-infrared 2–5 μm heterojunction laser diodes, in: I.T. Sorokina, K.L. Vodopyanov (Eds.), Solid-State Mid-Infrared Sources, in: Topics in Applied Physics, vol. 89, Springer, Berlin, Heidelberg, 2003, pp. 1–59.
[49] D.Z. Garbuzov, H. Lee, V. Khalfin, R. Martinelli, J.C. Connolly, G.L. Belenky, 2.3–2.7 μm room temperature CW operation of InGaAsSb–AlGaAsSb broad waveguide SCH-QW diode lasers, IEEE Photon. Technol. Lett. 11 (1999) 794–796.
[50] H.K. Choi, G.W. Turner, S.J. Eglash, High-power GaInAsSb–AlGaAsSb multiple-quantum-well diode lasers emitting at 1.9 μm, IEEE Photon. Technol. Lett. 6 (1994) 7–9.
[51] D.Z. Garbuzov, R.U. Martinelli, H. Lee, R.J. Menna, P.K. York, L.A. DiMarco, M.G. Harvey, R.J. Matarese, S.Y. Narayan, J.C. Connolly, 4 W quasi-continuous-wave output power from 2 μm AlGaAsSb/InGaAsSb single-quantum-well broadened waveguide laser diodes, Appl. Phys. Lett. 70 (1997) 2931–2933.
[52] J.G. Kim, L. Shterengasa, R.U. Martinelli, G.L. Belenky, D.Z. Garbuzov, W.K. Chan, Room-temperature 2.5 μm InGaAsSb/AlGaAsSb diode lasers emitting 1 W continuous waves, Appl. Phys. Lett. 81 (2002) 3146–3148.
[53] M. Garcia, A. Salhi, A. Pérona, Y. Rouillard, C. Sirtori, X. Marcadet, C. Alibert, Low threshold high-power room-temperature continuous-wave operation diode laser emitting at 2.26 μm, IEEE Photon. Technol. Lett. 16 (2004) 1253–1255.
[54] G.L. Belenky, J.G. Kim, L. Shterengas, A. Gourevitch, R.U. Martinelli, High-power 2.3 μm laser arrays emitting 10 W CW at room temperature, Electron. Lett. 40 (2004) 737–738.
[55] M.T. Kelemen, J. Weber, M. Rattunde, G. Kaufel, J. Schmitz, R. Moritz, M. Mikulla, J. Wagner, High-power 1.9 μm diode laser arrays with reduced far-field angle, IEEE Photon. Technol. Lett. 18 (2006) 628–630.
[56] H.K. Choi, J.N. Walpole, G.W. Turner, M.K. Connors, L.J. Missaggia, M.J. Manfra, GaInAsSb–AlGaAsSb tapered lasers emitting at 2.05 μm with 0.6-W diffraction-limited power, IEEE Photon. Technol. Lett. 10 (1998) 938–940.
[57] C. Pfahler, G. Kaufel, M.T. Kelemen, M. Mikulla, M. Rattunde, J. Schmitz, J. Wagner, GaSb-based tapered diode lasers at 1.93 μm with 1.5-W nearly diffraction-limited power, IEEE Photon. Technol. Lett. 18 (2006) 758–760.
[58] J.N. Walpole, H.K. Choi, L.J. Missaggia, Z.L. Liau, M.K. Connors, G.W. Turner, M.J. Manfra, C.C. Cook, High-power high-brightness GaInAsSb–AlGaAsSb tapered laser arrays with anamorphic collimating lenses emitting at 2.05 μm, IEEE Photon. Technol. Lett. 11 (1999) 1223–1225.
[59] E. Geerlings, M. Rattunde, J. Schmitz, G. Kaufel, H. Zappe, J. Wagner, Widely tunable GaSb-based external cavity diode laser emitting around 2.3 μm, IEEE Photon. Technol. Lett. 18 (2006) 1913–1915.
[60] M. Hümmer, K. Rößner, A. Benkert, A. Forchel, GaInAsSb–AlGaAsSb distributed feedback lasers emitting near 2.4 μm, IEEE Photon. Technol. Lett. 16 (2004) 380–382.
[61] C. Sirtori, J. Nagle, Quantum cascade lasers: the quantum technology for semiconductor lasers in the mid-far-infrared, C. R. Physique 4 (2003) 639–648.
[62] D. Hofstetter, J. Faist, High performances quantum cascade lasers and their applications, in: I.T. Sorokina, K.L. Vodopyanov (Eds.), Solid-State Mid-Infrared Sources, in: Topics in Applied Physics, vol. 89, Springer, Berlin, Heidelberg, 2003, pp. 61–96.
[63] F. Capasso, C. Gmachl, R. Paiella, A. Tredicucci, A.L. Hutchinson, D.L. Sivco, J.N. Baillargeon, A.Y. Cho, H.C. Liu, New frontiers in quantum cascade lasers and applications, IEEE J. Sel. Topics Quantum Electron. 6 (2000) 931–947.
[64] I. Vurgaftman, J.R. Meyer, Analysis of limitations to wallplug efficiency and output power for quantum cascade lasers, J. Appl. Phys. 99 (2006) 123108.
[65] S. Slivken, Z. Huang, A. Evans, M. Razeghi, High-power ($\lambda \simeq 9$ μm) quantum cascade lasers, Appl. Phys. Lett. 80 (2002) 4091–4093.
[66] S. Forget, C. Faugeras, J.-Y. Bengloan, M. Calligaro, O. Parillaud, M. Giovannini, J. Faist, C. Sirtori, High-power spatial singlemode quantum cascade lasers at 8.9 μm, Electron. Lett. 41 (2005) 418–419.
[67] D. Hofstetter, M. Beck, T. Aellen, J. Faist, U. Oesterle, M. Ilegems, E. Gini, H. Melchior, Continuous wave operation of a 9.3 μm quantum cascade laser on Peltier cooler, Appl. Phys. Lett. 78 (2001) 1964–1966.
[68] J.S. Yu, S. Slivken, A. Evans, L. Doris, M. Razeghi, High-power continuous-wave operation of a 6 μm quantum-cascade laser at room temperature, Appl. Phys. Lett. 83 (2003) 2503–2505.
[69] J.S. Yu, A. Evans, J. David, L. Doris, S. Slivken, M. Razeghi, Cavity-length effects of high-temperature high-power continuous-wave characteristics in quantum-cascade lasers, Appl. Phys. Lett. 83 (2003) 5136–5138.
[70] S. Blaser, High power and single frequency quantum cascade lasers for chemical sensing, in: 4th Workshop on Quantum Cascade Lasers, Technology and Applications, Freiburg, Germany, 2005.
[71] A. Evans, J.S. Yu, S. Slivken, M. Razeghi, Continuous-wave operation of $\lambda \simeq 4.8$ μm quantum cascade lasers, Appl. Phys. Lett. 85 (2004) 2166–2168.
[72] J.S. Yu, A. Evans, J. David, L. Doris, S. Slivken, M. Razeghi, High-power continuous-wave operation of quantum-cascade lasers up to 60 °C, IEEE Photon. Technol. Lett. 16 (2004) 747–749.
[73] A. Evans, J.S. Yu, S.J. David, L. Doris, K. Mi, S. Slivken, M. Razeghi, High-temperature, high-power, continuous-wave operation of buried heterostructure quantum-cascade lasers, Appl. Phys. Lett. 84 (2004) 314–316.
[74] J.S. Yu, A. Evans, S. Slivken, S.R. Darvish, M. Razeghi, Short wavelength ($\lambda \simeq 4.3$ μm) high-performance continuous-wave quantum-cascade lasers, IEEE Photon. Technol. Lett. 17 (2005) 1154–1156.
[75] W.W. Bewley, J.R. Lindle, C.S. Kim, I. Vurgaftman, J.R. Meyer, A.J. Evans, J.S. Yu, S. Slivken, M. Razeghi, Beam steering in high-power CW quantum-cascade lasers, IEEE J. Quantum Electron. 41 (2005) 833–841.
[76] C. Faugeras, S. Forget, E. Boer-Duchemin, H. Page, J.-Y. Bengloan, O. Parillaud, M. Calligaro, C. Sirtori, M. Giovannini, J. Faist, High-power room temperature emission quantum cascade lasers at $\lambda = 9$ μm, IEEE J. Quantum Electron. 41 (2005) 1430–1438.

[77] A. Evans, J. Nguyen, S. Slivken, J.S. Yu, S.R. Darvish, M. Razeghi, Quantum-cascade lasers operating in continuous-wave mode above 90 °C at $\lambda \simeq 5.25$ μm, Appl. Phys. Lett. 88 (2006) 051105.

[78] J.S. Yu, S. Slivken, A. Evans, S.R. Darvish, J. Nguyen, M. Razeghi, High-power $\lambda \simeq 9.5$ μm quantum-cascade lasers operating above room temperature in continuous-wave mode, Appl. Phys. Lett. 88 (2006) 091113.

[79] L. Diehl, D. Bour, S. Corzine, J. Zhu, G. Höfler, M. Lončar, M. Troccoli, F. Capasso, High-power quantum cascade lasers grown by low-pressure metal organic vapor-phase epitaxy operating in continuous wave above 400 K, Appl. Phys. Lett. 88 (2006) 201115.

[80] J.S. Yu, A. Evans, S. Slivken, S.R. Darvish, M. Razeghi, Temperature dependent characteristics of $\lambda \simeq 3.8$ μm room-temperature continuous-wave quantum-cascade lasers, Appl. Phys. Lett. 88 (2006) 251118.

[81] A. Wittmann, M. Giovannini, J. Faist, L. Hvozdara, S. Blaser, D. Hofstetter, E. Gini, Room temperature, continuous wave operation of distributed feedback quantum cascade lasers with widely spaced operation frequencies, Appl. Phys. Lett. 89 (2006) 141116.

[82] S. Slivken, A. Evans, W. Zhang, M. Razeghi, High-power, continuous-operation intersubband laser for wavelengths greater than 10 μm, Appl. Phys. Lett. 90 (2007) 151115.

[83] R. Maulini, D.A. Yarekha, J.-M. Bulliard, M. Giovannini, J. Faist, E. Gini, Continuous-wave operation of a broadly tunable thermoelectrically cooled external cavity quantum-cascade laser, Opt. Lett. 30 (2006) 2584–2587.

[84] K. Kennedy, A.B. Krysa, J.S. Roberts, K.M. Groom, R.A. Hogg, D.G. Revin, L.R. Wilson, J.W. Cockburn, High performance InP-based quantum cascade distributed feedback lasers with deeply etched lateral gratings, Appl. Phys. Lett. 89 (2006) 201117.

[85] C. Bauer, P. Geiser, J. Burgmeier, G. Holl, W. Schade, Pulsed laser surface fragmentation and mid-infrared laser spectroscopy for remote detection of explosives, Appl. Phys. B 85 (2006) 251–256.

[86] K.L. Vodopyanov, Mid-infrared optical parametric generator with extra-wide (3–19 μm) tunability: applications for spectroscopy of two-dimensional electrons in quantum wells, J. Opt. Soc. Am. B 16 (1999) 1579–1586.

[87] L.E. Myers, R.C. Eckardt, M.M. Fejer, R.L. Byer, W.R. Bosenberg, J.W. Pierce, Quasi-phase-matched optical parametric oscillators in bulk periodically poled $LiNbO_3$, J. Opt. Soc. Am. B 12 (1995) 2102–2116.

[88] K. Koch, G.T. Moore, E.C. Cheungy, Optical parametric oscillation with intracavity difference-frequency mixing, J. Opt. Soc. Am. B 12 (1995) 2268–2273.

[89] J.-M. Melkonian, A. Godard, M. Lefebvre, E. Rosencher, Pulsed optical parametric oscillators with intracavity optical parametric amplification: a critical study, Appl. Phys. B 86 (2007) 633–642.

[90] J.M. Fukumoto, H. Komine, W.H. Long Jr., E.A. Stappaerts, Periodically poled $LiNbO_3$ optical parametric oscillator with intracavity difference frequency mixing, in: W.R. Bosenberg, M.M. Fejer (Eds.), Trends in Optics and Photonics, in: Advanced Solid-State Lasers, vol. 19, Optical Society of America, 1998, pp. 245–248.

[91] B. Scherrer, I. Ribet, A. Godard, E. Rosencher, M. Lefebvre, Dual-cavity doubly resonant optical parametric oscillators: demonstration of pulsed single-mode operation, J. Opt. Soc. Am. B 17 (2000) 1716–1729.

[92] A. Desormeaux, M. Lefebvre, E. Rosencher, J.-P. Huignard, Mid-infrared high-resolution absorption spectroscopy by use of a semimonolithic entangled-cavity optical parametric oscillator, Opt. Lett. 29 (2004) 2887–2889.

[93] A. Berrou, A. Godard, E. Rosencher, M. Lefebvre, S. Spiekermann, Mid-IR entangled-cavity doubly resonant OPO pumped by a micro-laser, in: Conference on Lasers and Electro-Optics, Optical Society of America, 2007, Technical Digest, paper CThL6.

[94] A. Berrou, A. Godard, M. Lefebvre, Mid-IR entangled-cavity doubly resonant OPO pumped by a micro-laser, in: Conference on Lasers and Electro-Optics, Optical Society of America, 2007, Technical Digest, paper CThL6.

[95] H. Ishizuki, T. Taira, High-energy quasi-phase-matched optical parametric oscillation in a periodically poled MgO:$LiNbO_3$ device with a 5 mm × 5 mm aperture, Opt. Lett. 30 (2005) 2918–2920.

[96] G. Mennerat, P. Kupecek, High-energy narrow-linewidth tunable source in the mid infrared, in: W.R. Bosenberg, M.M. Fejer (Eds.), Trends in Optics and Photonics, in: Advanced Solid-State Lasers, vol. 19, Optical Society of America, 1998, pp. 269–272.

[97] J. Saikawa, M. Fujii, H. Ishizuki, T. Taira, 52 mJ narrow-bandwidth degenerated optical parametric system with a large-aperture periodically poled MgO:$LiNbO_3$ device, Opt. Lett. 31 (2006) 3149–3151.

[98] J. Saikawa, M. Miyazaki, M. Fujii, H. Ishizuki, T. Taira, Difference frequency generation in a $ZnGeP_2$ crystal pumped by a large aperture periodically poled MgO:$LiNbO_3$ optical parametric system, in: Advanced Solid-State Photonics 2007, The Optical Society of America, Washington, 2007, Technical Digest, MB8.

[99] M. Henriksson, M. Tiihonen, V. Pasiskevicius, F. Laurell, $ZnGeP_2$ parametric oscillator pumped by a linewidth-narrowed parametric 2 μm source, Opt. Lett. 31 (2006) 1878–1880.

[100] S. Nicolas, Ø. Nordseth, G. Rustad, G. Arisholm, High-energy mid-IR source based on two-stage conversion from 1.06 μm, in: C. Denman, I.T. Sorokina (Eds.), Trends in Optics and Photonics, in: Advanced Solid-State Photonics, vol. 98, Optical Society of America, 2005, pp. 417–422.

[101] R.K. Shori, Recent developments in scaling output energy from erbium-based lasers and their uses as pump sources for MWIR & LWIR OPOs, in: Laser and Electro-Optics Society Annual Meeting 2004 Conference Proceedings, vol. 2, IEEE, 2004, pp. 805–806.

[102] T.H. Allik, J.L. Ahl, S. Chandra, J.A. Hutchinson, W.W. Hovis, J. Fox, L. Newman, Refinements and additional characterization of an 8–12 μm tandem OPO design, in: M. Fejer, H. Injeyan, U. Keller (Eds.), Trends in Optics and Photonics, in: Advanced Solid-State Lasers, vol. 26, Optical Society of America, 1999, pp. 525–528.

[103] R.K. Shori, O.M. Stafsudd, N.S. Prasad, G. Catella, High energy $AgGaSe_2$ optical parametric oscillator operating in 5.7–7 μm region, in: Nonlinear Optics: Materials, Fundamentals, and Applications, 2000, pp. 179–181, Technical Digest.

[104] S. Chandra, T.H. Allik, G. Catella, J.A. Hutchinson, Tunable output around 8 μm from a single step $AgGaS_2$ OPO pumped at 1.064 μm, in: W.R. Bosenberg, M.M. Fejer (Eds.), Trends in Optics and Photonics, in: Advanced Solid-State Lasers, vol. 19, Optical Society of America, 1998, pp. 282–284.

[105] P.G. Schunemann, S.D. Setzler, L. Mohnkern, T.M. Pollak, D.F. Bliss, D. Weyburne, K. O'Hearn, 2.05-μm-laser-pumped orientation-patterned gallium arsenide (OPGaAs) OPO, in: Conference on Lasers and Electro-Optics, Optical Society of America, 2005, Technical Digest, paper CThQ4.
[106] P.G. Schunemann, Advances in NLO crystals for infrared parametric sources, Oral presentation given at Journées Scientifiques de l'ONERA (2007).
[107] P.A. Budni, M.G. Knights, E.P. Chicklis, K.L. Schepler, Kilohertz $AgGaSe_2$ optical parametric oscillator pumped at 2 μm, Opt. Lett. 18 (1993) 1068–1070.
[108] K.L. Vodopyanov, F. Ganikhanov, J.P. Maffetone, I. Zwieback, W. Ruderman, $ZnGeP_2$ optical parametric oscillator with 3.8–12.4 μm tunability, Opt. Lett. 25 (2000) 841–843.
[109] T.H. Allik, S. Chandra, D.M. Rines, P.G. Schunemann, J.A. Hutchinson, R. Utano, Tunable 7–12 μm optical parametric oscillator using a Cr,Er:YSGG laser to pump CdSe and $ZnGeP_2$ crystals, Opt. Lett. 22 (1997) 597–599.
[110] Y. Isyanova, A. Dergachev, D. Welford, P.F. Moulton, Multi-wavelength, 1.5–10 μm tunable, tandem OPO, in: M. Fejer, H. Injeyan, U. Keller (Eds.), Trends in Optics and Photonics, in: Advanced Solid-State Lasers, vol. 26, Optical Society of America, 1999, pp. 548–553.
[111] K.L. Vodopyanov, O. Levi, P.S. Kuo, T.J. Pinguet, J.S. Harris, M.M. Fejer, B. Gerard, L. Becouarn, E. Lallier, Optical parametric oscillation in quasi-phase-matched GaAs, Opt. Lett. 29 (2004) 1912–1914.
[112] S.E. Bisson, T.J. Kulp, O. Levi, J.S. Harris, M.M. Fejer, Long-wave IR chemical sensing based on difference frequency generation in orientation-patterned GaAs, Appl. Phys. B 85 (2006) 199–206.